

UNIVERSIDADE ESTADUAL DE CAMPINAS

Faculdade de Engenharia Mecânica

ANDREZA COSTA

Global chemical kinetics mechanisms for renewable fuels including supercritical combustion with real gas equation of state

Mecanismos globais de cinética química para combustíveis renováveis incluindo combustão supercrítica com equação de estado de gás real

CAMPINAS

ANDREZA COSTA

Global chemical kinetics mechanisms for renewable fuels including supercritical combustion with real gas equation of state

Mecanismos globais de cinética química para combustíveis renováveis incluindo combustão supercrítica com equação de estado de gás real

Dissertation presented to the School of Mechanical Engineering of the University of Campinas in partial fulfillment of the requirements for the degree of Master in Mechanical Engineering in the area of Thermal and Fluids.

Dissertação apresentada à Faculdade de Engenharia Mecânica da Universidade Estadual de Campinas como parte dos requisitos exigidos para a obtenção do título de Mestra em Engenharia Mecânica na área de Térmica e Fluidos.

Orientador: Prof. Dr. Rogério Gonçalves dos Santos

ESTE TRABALHO CORRESPONDE À VERSÃO FINAL DA DISSERTAÇÃO DEFENDIDA PELA ALUNA ANDREZA COSTA, E ORIENTADA PELO PROF. DR. ROGÉRIO GONÇALVES DOS SANTOS.

CAMPINAS

Ficha catalográfica Universidade Estadual de Campinas (UNICAMP) Biblioteca da Área de Engenharia e Arquitetura Vanessa Evelyn Costa - CRB 8/8295

Costa, Andreza, 1998-

C823g

Global chemical kinetics mechanisms for renewable fuels including supercritical combustion with real gas equation of state / Andreza Costa. – Campinas, SP: [s.n.], 2025.

Orientador: Rogério Gonçalves dos Santos. Dissertação (mestrado) – Universidade Estadual de Campinas (UNICAMP), Faculdade de Engenharia Mecânica.

1. Combustão. 2. Cinética química. 3. Fluídos supercríticos. 4. Etanol. 5. Hidrogênio. I. Santos, Rogério Gonçalves dos, 1978-. II. Universidade Estadual de Campinas (UNICAMP). Faculdade de Engenharia Mecânica. III. Título.

Informações complementares

Título em outro idioma: Mecanismos globais de cinética química para combustíveis renováveis incluindo combustão supercrítica com equação de estado de gás real **Palavras-chave em inglês:**

Combustion Chemical kinetics Supercritical fluids Ethanol Hydrogen

Área de concentração: Térmica e Fluidos **Titulação:** Mestra em Engenharia Mecânica

Banca examinadora:

Rogério Gonçalves dos Santos [Orientador]

Ingrid Lopes Motta Leonel Rincón Cancino **Data de defesa:** 29-08-2025

Programa de Pós-Graduação: Engenharia Mecânica

Objetivos de Desenvolvimento Sustentável (ODS)

ODS: 7. Energia acessível e limpa

ODS: 13. Ação contra a mudança global do clima

Identificação e informações acadêmicas do(a) aluno(a)

- ORCID do autor: https://orcid.org/0009-0002-5894-8577

- Currículo Lattes do autor: https://lattes.cnpq.br/1377763285722697

Rogério Gonçalves dos Santos

Ingrid Lopes Motta

Leonel Rincón Cancino

A Ata de Defesa com as respectivas assinaturas dos membros encontra-se no SIGA/Sistema de Fluxo de Dissertação/Tese e na Secretaria do Programa da Unidade.

ACKNOWLEDGMENTS

To my mother, Angelita Rosa, my father, Gilmar Costa, and my sister, Camila Costa, to whom I am grateful and proud.

To my advisor, Prof. Dr. Rogério Gonçalves dos Santos, I am thankful for the opportunity of this journey, for the guidance, dedication, and support.

To my friends, Dayane Silva and Jacqueline Lembo, I am grateful for their companionship throughout this time.

To my love, Danilo Bueno Machado, for bringing light to my life.

To the professors, Prof. Dr. Ingrid Motta, Prof. Dr. Leonel Rincón Cancino, Prof. Dr. Arnaldo Walter, Prof. Dr. Guilherme Fraga, and Prof. Dr. Caio Rufino, who were part of my master's journey and continue to inspire me to pursue this career.

This study was financed in part by the Coordenação de Aperfeiçoamento de Pessoal de Nível Superior (CAPES) – Finance Code 001, and Fundação de Desenvolvimento da Pesquisa (FUNDEP), Rota 2030 (Project 27192*6) - Linha V.

RESUMO

Em simulações de escoamentos reativos, mecanismos de cinética química detalhados descrevem as reações químicas elementares da combustão. Devido ao grande número de espécies e reações, o custo computacional é elevado no acoplamento desses mecanismos com algoritmos que resolvem as equações do transporte em escoamentos turbulentos e em geometrias complexas. Mecanismos globais de cinética química otimizados permitem redução considerável do custo computacional, um dos principais problemas em simulações de grandes escalas da turbulência (Large Eddy Simulations - LES) e em simulações numéricas diretas (Direct Numerical Simulations - DNS). Em ultra-alta pressão, a hipótese de gás ideal resulta em discrepâncias em prever o comportamento de fluido supercrítico. Mecanismos globais de cinética química em ultra-alta pressão, incluindo os efeitos de fluido real através de equação cúbica de estado, ainda não foram reportados na literatura. Esta dissertação propõe novos mecanismos globais para os combustíveis etanol e hidrogênio. Mecanismos globais de cinética química para hidrogênio supercrítico foram propostos utilizando a equação cúbica de estado de gás real de Peng-Robinson. A otimização foi realizada de acordo com um banco de dados de um mecanismo detalhado. Para o combustível etanol, foram obtidos mecanismos globais de duas etapas, que reproduziram velocidades de chama laminar com máximo de 10% de diferença e perfis de temperatura com máximo de 6% de diferença, em relação ao mecanismo detalhado, para pressão de 1 atm, temperatura de 428 K e razões de equivalência entre 0.6-1.8. Mecanismos globais para pressões entre 1-2 atm também foram obtidos, com desvio máximo de 20% para velocidades de chama e perfis de temperatura. Para o combustível hidrogênio, um mecanismo global de uma etapa foi obtido, com máximo de 20% de diferença para velocidade de chama laminar, em relação ao mecanismo detalhado, para pressão de 1 atm, temperatura de 300 K e razões de equivalência entre 0.5-5.0. Em ultra-alta pressão, os resultados obtidos utilizando-se da equação de estado de Peng-Robinson apresentou discrepâncias em relação à hipótese de gás ideal para velocidades de chama laminar, estrutura de chama, e atraso de tempo de ignição de hidrogênio. Para pressões entre 200-300 atm, temperatura de 300 K e razões de equivalência entre 0.6-3.0, os mecanismos de uma etapa reproduziram velocidades de chama laminar com diferença máxima de 20% em relação ao mecanismo detalhado. Os mecanismos globais de cinética químicas obtidos demonstram potencial para modelar combustão em condições atmosféricas e em ultra-alta pressão, principalmente em simulações numéricas onde a descrição detalhada se torna proibitiva.

Palavras-chave: combustão, cinética química, chama laminar, fluido supercrítico

ABSTRACT

In reactive flow simulations, detailed chemical kinetics mechanisms describe the combustion elementary chemical reactions. Due to the large number of species and reactions, a high computational cost is achieved when coupling these mechanisms with algorithms that solve the transport equations in turbulent flows and complex geometries. Optimized global chemical kinetics mechanisms allow for a considerable computational cost reduction, a major issue when dealing with Large Eddy Simulations (LES) and Direct Numerical Simulations (DNS). Under ultra-high pressure, the ideal gas assumption may lead to discrepancies in predicting the supercritical fluid behavior. Global chemical kinetics mechanisms under ultra-high pressure conditions, including real-fluid effects through a cubic equation of state, have not yet been reported in the literature. This dissertation proproses new global mechanisms for ethanol and hydrogen fuels. Global chemical kinetics mechanisms for supercritical hydrogen were proposed using the real gas Peng-Robinson cubic equation of state. The optimization was performed according to the database of a detailed mechanism. For ethanol fuel, two-step global mechanisms were obtained, which predicted laminar flame speeds with maximum 10% difference, and temperature profiles with maximum 6% difference, relative to the detailed mechanism at a pressure of 1 atm, temperature of 428 K, and over the equivalence ratio range 0.6-1.8; global mechanisms at pressures of 1-2 atm were also obtained, with maximum 20% difference for laminar flame speeds and temperature profiles. For hydrogen fuel, a one-step mechanism was obtained, with maximum 20% difference in laminar flame speeds, relative to the detailed mechanism, at a pressure of 1 atm, temperature of 300 K, and over the equivalence ratio range 0.5-5.0. Under ultra-high pressure, the results obtained utilizing the Peng-Robinson equation of state presented discrepancies from the ideal gas assumption for hydrogen laminar flame speeds, flame structure, and ignition delay times. At pressures of 200-300 atm, temperature of 300 K, and over the equivalence ratio range 0.6-3.0, the one-step mechanisms predicted laminar flame speeds with maximum 20% difference relative to the detailed mechanism. The obtained global chemical kinetics mechanisms demonstrates potential to model combustion under atmospheric and ultra-high-pressure conditions, mainly for numerical simulations in which the detailed description becomes prohibitive.

Keywords: combustion, chemical kinetics, laminar flame, supercritical fluid

LIST OF FIGURES

Figure 1.1 -	- Earth's average surface temperature data from 1880 (pre-industrial) to 2024.	
	Source: NATIONAL AERONAUTICS AND SPACE ADMINISTRATION	
	(NASA) (2024)	19
Figure 1.2 -	- Joint Research Center (JRC) emissions database for global atmospheric research	
	GHG emissions of all world countries per year in gigatonnes of equivalent	
	carbon dioxide ($GtCO_{2,eq}$) and equivalent tonne carbon dioxide per capita	
	(tCO _{2,eq/cap}). Source: CRIPPA et al. (2024)	20
Figure 2.1 –	- GRI 3.0 detailed chemical kinetics mechanism. All reactions are available	
	in SMITH et al. (2000)	26
Figure 2.2 -	- Stoichiometric methane-air flame strucure at $P=1$ atm and $T_u=300~{\rm K}$	
	with the Gri 3.0 (SMITH et al., 2000) chemical kinetics mechanism	29
Figure 2.3 -	-Ignition delay time according to the OH* radical mass fraction. Source:	
	Adapted from Goodwin et al. (2025)	30
Figure 2.4 -	- Phase diagram. Source: Gupta et al. (2014)	34
Figure 3.1 -	- Flowchart to obtain reaction orders for the two-step ethanol chemical kinetics	
	mechanism.	39
Figure 3.2 -	Three runs of the optimization method for (a) $\phi=0.6$, (b) $\phi=1.1$ and (c)	
	$\phi = 1.2. \dots $	40
Figure 3.3 -	- Ethanol-air premixed laminar flame speed at $P=1$ atm and $T_u=428~{\rm K.}$	41
Figure 3.4 -	- Comparison between temperature profiles of the two-step and detailed ethanol	
	chemical kinetics mechanisms for $\phi=0.6$ to 1.1 at $P=1$ atm and $T_u=428$	
	K	42
Figure 3.5 -	- Comparison between temperature profiles of the two-step and detailed ethanol	
	chemical kinetics mechanisms for $\phi=1.2$ to 1.8 at $P=1$ atm and $T_u=428$	
	K	43
Figure 3.6 -	- Laminar flame speed comparison for different unburned gas temperatures	
	between chemical kinetics mechanisms (lines) and experimental data (markers),	
	for stoichiometric mixtures and $P = 1$ atm	44

Figure 3.7 -	- Pressure exponent for the reference pressure of 1 atm, for (a) kerosene fuel,	
	$P=2$ to 12 atm, $T_u=300$ K, and detailed chemical kinetics mechanism of	
	LUCHE (2003), and (b) ethanol fuel, $P=2$ to 10 atm, $T_u=428$ K, detailed	
	mechanism of PLÁCIDO et al. (2024)	45
Figure 3.8 -	- Laminar flame speed for $T_u=428~{\rm K},$ (a) $P=1~{\rm atm}$ and (b) $P=2~{\rm atm},$	
	according to the equivalence ratio	46
Figure 3.9 -	- Reaction orders for the two optimized sets of parameters according to the	
	equivalence ratio	47
Figure 3.10	-Comparison between temperature profiles of the two-step mechanism optimized	
	for $P=1$ and 2 atm and detailed ethanol chemical kinetics mechanisms, for	
	$\phi=0.6$ to 1.1 at $P=1$ atm and $T_u=428$ K	48
Figure 3.11	-Comparison between temperature profiles of the two-step mechanism optimized	
	for $P=1$ and 2 atm and detailed ethanol chemical kinetics mechanisms for	
	$\phi=1.2$ to 1.8 at $P=1$ atm and $T_u=428$ K	49
Figure 4.1 -	- Laminar flame speeds for hydrogen-air premixed flames at $T_u=300~\mathrm{K}$ and	
	P=1 to 100 atm	52
Figure 4.2 -	-OH* (a), H* (b), and O* (c) species profiles for H ₂ -air laminar preximed	
	flames at $T_u=300$ K and $P=1$ to 100 atm	52
Figure 4.3 -	$-H_2O_2$ (a) and HO_2^* (b) species profiles for H_2 -air laminar premixed flames at	
	$T_u=300~{ m K}$ and $P=1$ to 100 atm	53
Figure 4.4 -	- Sensitivity coefficient for stoichiometric laminar flame speeds of H ₂ -air at	
	$T_u = 300$ K and $P = 1$ to 100 atm, Li et al. (2004) chemical kinetics	
	mechanism.	53
Figure 4.5 -	- Ignition delay times for stoichiometric H_2 -air mixtures at $P=1$ to 100 atm.	54
Figure 4.6 -	- Laminar flame speeds of H_2 -air mixtures for $T_u=373$ K, $P=150$ and 300	
	atm, comparing IG EoS and PR EoS	56
Figure 4.7 -	- Laminar flame speeds of H_2 -air mixtures for $T_u=373$ K, $P=200$ and 400	
	atm, comparing IG EoS and PR EoS	56
Figure 4.8 -	- Ignition delay time simulations for stoichiometric H_2 -air flames at $P=100$	
	and 300 atm, $T_i=870$ to 1250 K, comparing IG EoS and PR EoS	57
Figure 4.9 -	- Ignition delay time simulations for stoichiometric H_2 -air flames at $P=150$	
	and 400 atm. $T_i = 870$ to 1250 K, comparing IG EoS and PR EoS.	57

Figure 4.10-	-Mixture gas density and temperature profiles of H ₂ -air stoichiometric flames	
	for $T_u = 373$ K, $P = 400$ atm, comparing IG EoS and PR EoS	58
Figure 4.11-	-O* and H* mass fraction profiles of H ₂ -air stoichiometric flames for T_u =373	
	K, $P=400$ atm, comparing IG EoS and PR EoS	59
Figure 4.12-	-H ₂ O ₂ and OH* mass fraction profiles of H ₂ -air stoichiometric flames for	
	$T_u=373$ K, $P=400$ atm, comparing IG EoS and PR EoS	59
Figure 4.13-	-Genetic algorithm flowchart. Source: GAD (2018)	61
Figure 4.14-	-Premixed hydrogen-air laminar flame speeds at $T_u=300~{\rm K}$ and $P=1$ atm.	62
Figure 4.15-	-Premixed hydrogen-air laminar flame speeds at $P=1$ atm and $T_u=100$ to	
	600 K	62
Figure 4.16-	-Premixed hydrogen-air laminar flame speeds at $T_u=300~{\rm K}$ and $P=250$	
	atm	63
Figure 4.17-	-Premixed hydrogen-air laminar flame speeds at $T_u=300~{\rm K}$ and $P=200$	
	atm	64
Figure 4.18-	-Premixed hydrogen-air laminar flame speeds at $T_u = 300$ K and $P = 300$	
	atm	65
Figure 4.19-	-Pre-exponential factor of the global kinetic mechanisms for $P=200,250,$	
	and 300 atm	65
Figure 4.20-	-Premixed hydrogen-air flame structure at $T_u=300~{\rm K}$ and $P=250~{\rm atm}$ for	
	(a, b) $\phi = 0.6$, (c, d) $\phi = 1.0$, and (e, f) $\phi = 3.0$	66
Figure 4.21-	-Premixed hydrogen-air heat release rate profiles at $T_u=300~{\rm K}$ and $P=250$	
	atm for (a) $\phi=0.6$, (b) $\phi=1.0$, and (c) $\phi=3.0$	67
Figure 4.22-	-Premixed hydrogen-air ignition delay time at $P=250$ atm for (a) $\phi=0.6$,	
	(b) $\phi=1.0$, and (c) $\phi=3.0$	67

LIST OF TABLES

Table 1.1 – Annual world fuel ethanol production (Mil. Gal.)	21
Table 2.1 – Time and spatial scales associated with the physical phenomena present in	
combustion chambers	31
Table 2.2 – Critical properties	34
Table 3.1 – Two-step ethanol chemical kinetics mechanism parameters for $P=1$ atm,	
$\phi=0.6$ to $\phi=1.8.$	41
Table 3.2 – Reactant order obtained through Equation 3.13 and the detailed mechanism	
of PLÁCIDO et al. (2024) for $T_u=428$ K, $P^0=1$ atm, and $P=2$ atm	45
Table 3.3 – Optimized two-step ethanol mechanism parameters for $P=1$ and 2 atm,	
$\phi=0.6$ to $\phi=1.8.$	46
Table 4.1 – Detailed chemical kinetics mechanisms utilized in this dissertation	51
Table 4.2 – Global chemical kinetics mechanism for H_2 -air at $T_u = 300$ K and $P = 1$ atm.	61
Table 4.3 – Global chemical kinetics mechanisms for H_2 -air at $T_u = 300$ K and $P = 250$	
atm	63
Table 4.4 – Global chemical kinetics mechanisms for H_2 -air at $T_u = 300$ K and $P = 200$	
atm	64
Table 4.5 – Global chemical kinetics mechanisms for H_2 -air at $T_u = 300$ K and $P = 300$	
atm.	64

LIST OF ABBREVIATIONS AND ACRONYMS

LES Large-Eddy Simulation

DNS Direct numerical aimulation

NASA National Aeronautics and Space Administration

JRC Joint Research Center

1-D One-dimensional

UHCs Unburned Hydrocarbons

EGR Exhaust gas recirculation

LFS Laminar flame speed

IDT Ignition delay time

HRR Heat release rate

EoS Equation of state

IG Ideal gas

PR Peng-Robinson

LIST OF SYMBOLS

\mathcal{O}	Order of				
$GtCO_{2,eq}$	Gigatonnes of equivalent carbon dioxide				
$tCO_{2,eq/cap}$	Equivalent tonne of carbon dioxide per capita				
ϕ	Equivalence ratio				
Y	Mass fraction				
F	Fuel subscript				
O	Oxidizer subscript				
stq	Stoichiometric subscript				
ν'	Stoichiometric coefficient				
W	Molecular weight	[kg/mol]			
x	Coordinate				
u	Axial velocity component	[m/s]			
s_L	Laminar flame speed	[m/s]			
ho	Density	$[kg/m^3]$			
\dot{m}''	Mass flux	$[kg/(m^2s)]$			
∂	Partial derivative				
$\dot{\omega}$	Molar production rate	$\left[\frac{\text{mol}}{\text{m}^3\text{s}}\right]$			
T	Temperature	[K]			
P	Thermodinamic pressure	[atm]			
\mathcal{R}	Universal gas constant	$\left[\frac{J}{K.mol}\right]$			
n, i	Species indexes				
N	Total number of species				
r	Reaction index				
R	Total number of reactions				
c_p	Heat capacity at constant pressure	$\left\lceil \frac{J}{\text{kg.K}} \right\rceil$			
h	Specific enthalpy	[J/kg]			
μ	Dynamic viscosity	$\left[\frac{\mathrm{kg}}{\mathrm{m.s}}\right]$			
λ	Thermal conductivity	$\left[\frac{W}{m.K}\right]$			
X	Molar fraction				

$ar{W}$	Mixture mean molecular weight	[kg/mol]
\mathcal{N}	Symbol representing a species	
e	Euler number	
k_f	Forward reaction rate coefficient	
k_b	Backward reaction rate coefficient	
[X]	Molar concentration	[mol/m ³]
A	Pre exponential factor	$\left\lceil \frac{m^3}{\text{mol}^{p-1}s} \right\rceil$
E_a	Activation energy	[J/mol]
$E_{a,g}$	Global activation energy	[J/mol]
β	Temperature exponent	
ΔS^0	Change in the reference state entropy	[J/K]
H	Molar enthalpy	[J/mol]
ΔH^0	Change in the reference state molar enthalpy	[J/mol]
m	Mass	[kg]
\dot{m}_{in}	Mass flow rate entering the control volume	[kg/s]
\dot{m}_{out}	Mass flow rate leaving the control volume	[kg/s]
\dot{m}_{wall}	Mass flow rate produced on the surface	[kg/s]
\dot{m}_{gen}	Mass flow rate generated on the surface	[kg/s]
\dot{Q}	Heat rate added to the control volume	[J/s]
U	Total internal energy	[J]
a	NASA-7 polynomial coefficient	
t	Time	[s]
d	Total derivative	
α	Peng-Robinson attraction parameter	
b	Van der Waals repulsive volume correction	
κ	Peng-Robinson parameter	
ω	Accentric factor	
V	Volume	$[m^3]$
P_c	Critical pressure	[atm]
T_c	Critical temperature	[K]
$oldsymbol{x}$	Array containing the spatial grid in x direction	[m]
T(x)	Array containing the temperature profile	[K]

n_F	Fuel reaction order	
n_O	Oxidizer reaction order	
c	Correction function	
g	Correction function	
T^0	Reference temperature	[K]
P^0	Reference pressure	[atm]
T_u	Unburned gas temperature	[K]
ln	Natural logarithm	
α_P	Pressure exponent	
α_T	Temperature exponent	
ε	Relative difference	
dtl	Detailed mechanism subscript	
f	Fitness function	
w	Laminar flame speed weight	

CONTENTS

1	INT	RODUCTION	19
	1.1	Context	19
	1.2	Objectives	22
	1.3	Publications related to this dissertation	22
	1.4	Dissertation organization	23
2	LIT	ERATURE REVIEW	24
	2.1	Chemical kinetics	24
	2.2	Laminar premixed flame	27
	2.3	Ignition delay time	29
	2.4	Global chemical kinetics mechanisms	30
	2.5	Supercritical combustion	33
3	ETH	HANOL	36
	3.1	Methods	36
	3.2	Results	39
4	HYI	DROGEN	51
	4.1	Kinetics of high-pressure hydrogen flames	51
		4.1.1 Methods	51
		4.1.2 Results	51
	4.2	Supercritical combustion with real gas equation of state	55
		4.2.1 Methods	55
		4.2.2 Results	55
	4.3	Global chemical kinetics mechanisms	60
		4.3.1 Methods	60
		4.3.2 Results	61
5	CO	NCLUSIONS AND FUTURE WORKS	68
	5.1	Conclusions	68
	5.2	Future works	69
Bi	bliog	raphy	70

1 INTRODUCTION

1.1 Context

The extensive emission of greenhouse gases by human activities has led to the overheating of the Earth. Climate change-related events such as extreme hot and extreme low temperatures, heatwaves, floods, and wildfires are more often, which threaten the habitable conditions. Concerning on that, the Paris agreement was estabilished in 2015 between 196 nations, with the goal to keep the average temperature in maximum 1.5°C above pre-industrial levels (1850-1900) (UNITED NATIONS CLIMATE CHANGE, 2024). However, this limit is getting close: according to the latest data, the increase of the mean temperature achieved in 2024 its higher average of 1.28 °C above the pre-industral levels (Figure 1.1), and the increase of greenhouse gas emissions among all the anthropogenic activity sectors is noticed (Figure 1.2). In this scenario, it is essential to considerably reduce the emissions to preserve the climate. The most expressive emissions are of carbon dioxide (CO₂) provenient from power industry, industrial combustion, and transport (CRIPPA *et al.*, 2024). The transition to renewable fuels is necessary to defossilize the energy sector, thereby reducing the CO₂ emissions during fossil fuels burning.

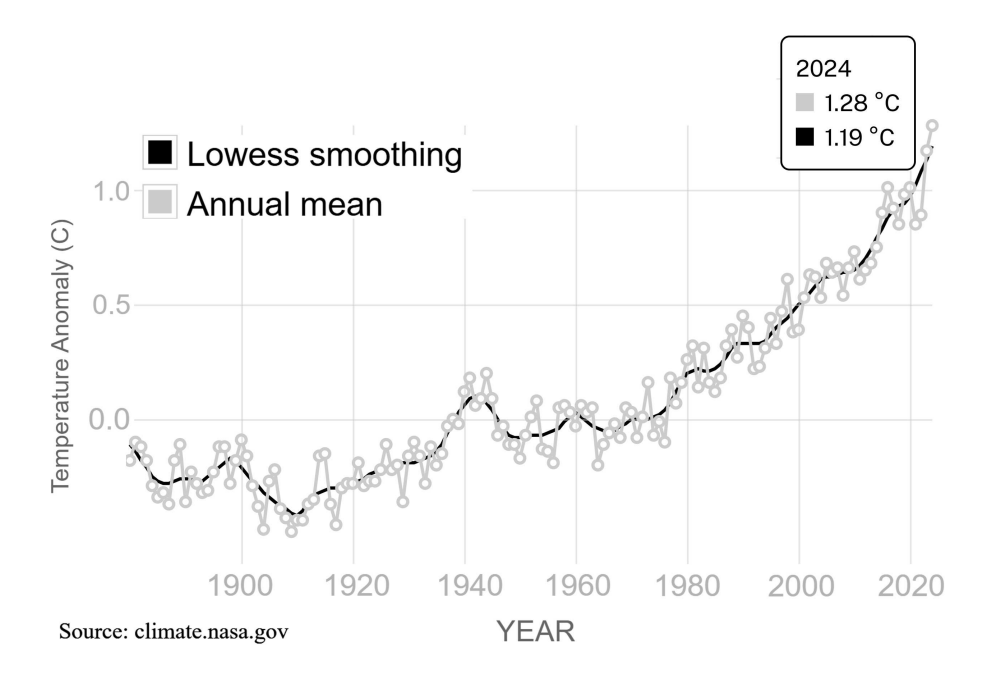


Figure 1.1 – Earth's average surface temperature data from 1880 (pre-industrial) to 2024. Source: NATIONAL AERONAUTICS AND SPACE ADMINISTRATION (NASA) (2024).

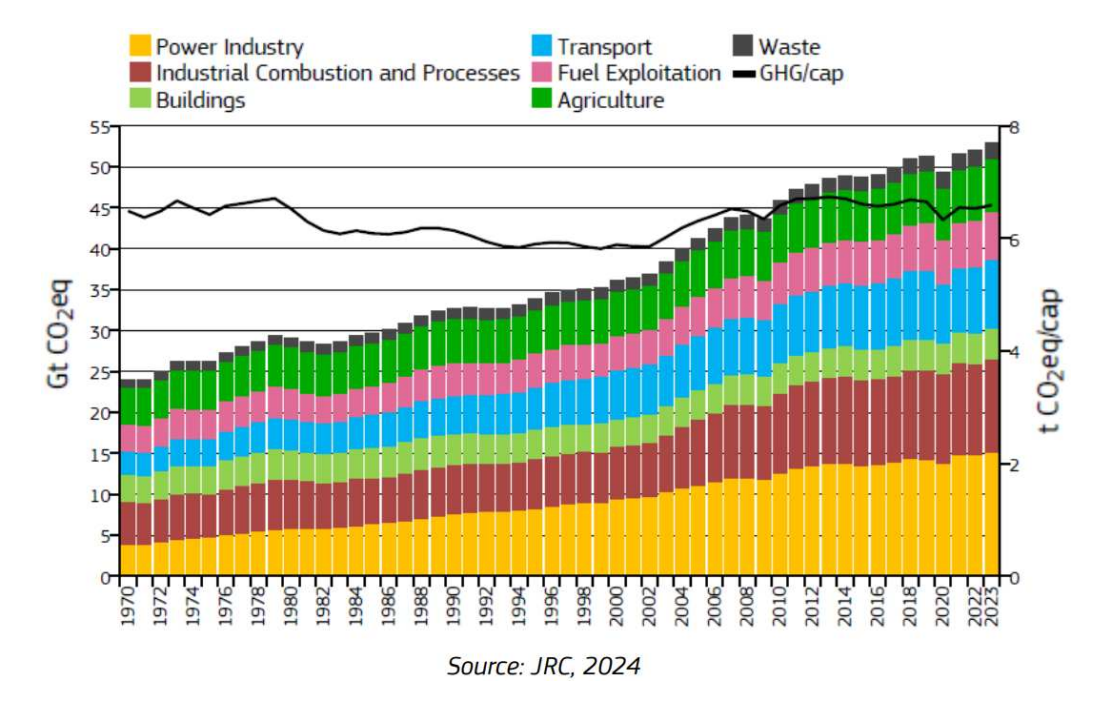


Figure 1.2 – Joint Research Center (JRC) emissions database for global atmospheric research GHG emissions of all world countries per year in gigatonnes of equivalent carbon dioxide (GtCO_{2,eq}) and equivalent tonne carbon dioxide per capita (tCO_{2,eq/cap}). Source: CRIPPA *et al.* (2024).

Hydrogen (H₂) it a carbon-free potential renewable fuel, considered an energy carrier due its high energy density per mass. Its clean burning emits mainly water vapor, and has potential for large-scale green production through water electrolysis using renewable electricity, such as provenient from solar, wind, and hydro energy sources (ANAND *et al.*, 2025). Biofuels had also gained attention in the energy transition; the climate conditions in Brazil and vast territory allows for intense agriculture activities, including large sugarcane mills to produce sugar and ethanol (C₂H₅OH) fuel. Brazil is the second largest producer of ethanol fuel, following the United States (Tab. 1.1), and the largest exporter, with growing consumption due to the flex-fuel vehicles fleet (WALTER *et al.*, 2011).

Table 1.1 – Annual world fuel ethanol production (Mil. Gal.).

Region	2020	2021	2022	2023	2024	% of World Production
United States	13941	15016	15361	15580	16219	52%
Brazil	8100	7320	7400	8470	8780	28%
India	530	950	1220	1510	1630	5%
European Union	1310	1380	1420	1390	1440	5%
China	940	900	960	1070	1200	4%
Canada	429	434	447	454	464	1%
Thailand	390	350	380	340	360	1%
Argentina	210	270	310	310	310	1%
Rest of World	630	690	722	806	807	3%
Total	26480	27310	28220	29930	31210	

Source: RENEWABLE FUELS ASSOCIATION (2025).

Combustion numerical simulations are essential for the development of efficient technologies with renewable fuels and to understand its behavior in different operation conditions. In the process of combustion, fuel and oxidizer molecules interact to form and consume chemical species. Detailed chemical kinetics mechanisms from dozens to hundreds of species and hundreds to thousands of elementary reactions have shown good agreement with experimental data in numerical simulations. The transport equations are solved for every time step and spatial grid point, as well the conservation of each species, that are coupled by all elementary reactions; however, the detailed chemistry description is computationally expensive for turbulent flows, complex geometries, and three-dimensional numerical simulations (POINSOT; VEYNANTE, 2005).

Optimization methods can be used to reduce the number of species and reactions while maintaining reasonable agreement with the key flow quantities obtained using the detailed chemical kinetics mechanism. One-step and two-step mechanisms, with rate parameters adjusted to replicate the outputs of the detailed chemistry, have been widely studied, particularly for hydrocarbons and hydrogen fuels. One of the first works on global mechanisms concerning the computational cost of the detailed description is presented by WESTBROOK and DRYER (1981), and their work is a reference for global chemical kinetics mechanisms studies; among them, FRANZELLI *et al.* (2010) introduced a two-step mechanism for kerosene fuel applicable across a wide range of pressures. Further efforts include the virtual chemistry framework presented by CAILLER (2018); through virtual intermediate and product species, the mechanism was capable of successfully reproducing the temperature profiles of a detailed

mechanism for methane fuel. KILDARE *et al.* (2024) proposed one-step mechanisms for hydrogen and methane fuels valid under high-pressure and high-temperature conditions, in which the hydrogen mechanism demonstrated the capability of a 100 times computational cost reduction for CFD turbulent simulations.

1.2 Objectives

The overall objective of this dissertation is to develop new global chemical kinetics mechanisms for ethanol an hydrogen renewable fuels, including the supercritical combustion of hydrogen through the Peng-Robinson equation of state. To achieve this, the following specific objectives are defined:

- Conducting a literature review on global chemical kinetics mechanisms;
- Implementing an algorithm in python programming language that recieves the detailed mechanism database as an input, and return as outputs, the optimal global mechanisms parameters;
- Studying ethanol chemical kinetics and obtain two-step global mechanisms;
- Studying hydrogen chemical kinetics with ideal gas and obtain a one-step mechanism at atmospheric conditions;
- Studying hydrogen kinetics with real gas and obtain one-step chemical kinetics mechanisms at high-pressure conditions.

1.3 Publications related to this dissertation

The results presented in this dissertation have led to the following publications in conference proceedings:

- Andreza Costa, Paulo Vitor Ribeiro Plácido, Rogério Gonçalves dos Santos. Two-step chemical mechanism for ethanol-air premixed flames. 20th Brazilian Congress of Thermal Sciences and Engineering, Foz do Iguaçu, Paraná, Brazil, 2024.
- Andreza Costa, Paulo Vitor Ribeiro Plácido, Rogério Gonçalves dos Santos. Kinetic mechanism for hydrogen flames under transcritical/supercritical state with real gas

- equation. 16th International Conference on Combustion Technologies for a Clean Environment, Lisbon, Portugal, 2025.
- Andreza Costa, Henrique B. Mantovani, Rogério Gonçalves dos Santos. Kinetics of High-Pressure Hydrogen Flames. 28th International Congress of Mechanical Engineering, Curitiba, Paraná, Brazil, 2025.

1.4 Dissertation organization

Chapter 2 presents bases about chemical kinetics, one-dimensional combustion modeling in steady state premixed laminar flames, and transient simulations in zero-dimensional constant volume reactors. A review on global mechanisms and supercritical combustion is also provided. The Chapter 3 presents the methodology and results about the two-step chemical kinetics mechanisms for ethanol fuel, calibrated from a database generated with recent ethanol-reduced mechanism, composed of 51 species and 627 reactions, developed in the study of PLÁCIDO *et al.* (2024) about gasoline/ethanol high-pressure combustion. Chapter 4 presents a review on laminar hydrogen flames under high-pressure, and also global mechanisms for hydrogen including supercritical combustion with the Peng-Robinson equation of state. In Chapter 5, conclusions and future works are discussed.

2 LITERATURE REVIEW

This chapter starts with a review on chemical kinetics in Section 2.1. As laminar flame speeds and ignition delay times are widely used to validate chemical kinetics mechanisms, Section 2.2 presents the fundamentals of laminar premixed flames, and Section 2.3 present the formulation of constant pressure reactors. In Section 2.4, a literature review on global chemical kinetics mechanisms is presented, followed by a review on supercritical combustion in Section 2.5.

2.1 Chemical kinetics

In the process of combustion, fuel and oxidizer molecules interact to form and consume new species through the formation and destruction of chemical bonds due to molecular collisions and molecular forces; chemical kinetics involves the study of the elementary reactions and the rate that they occur (TURNS, 1996).

Considering N species reacting through R reactions:

$$\sum_{n=1}^{N} \nu'_{n,r} \mathcal{N}_n \rightleftharpoons \sum_{n=1}^{N} \nu''_{n,r} \mathcal{N}_n, \quad r = 1, ..., R,$$
(2.1)

in which $\nu'_{n,r}$, $\nu''_{n,r}$ are the stoichiometric coefficients of species n and reaction r, and \mathcal{N} represents a species; mass conservation gives:

$$\nu_{n,r} = \nu_{n,r}'' - \nu_{n,r}'. \tag{2.2}$$

The production rate $(\dot{\omega})$ of species n is given by:

$$\dot{\omega}_n = W_n \sum_{r=1}^R \nu_{n,r} \left(k_{f,r} \prod_{n=1}^N [X_n]^{\nu'_{n,r}} - k_{b,r} \prod_{n=1}^N [X_n]^{\nu''_{n,r}} \right), \tag{2.3}$$

in which W is the molar weight, $[X_n]$ is the molar concentration, and $k_{f,r}$ and $k_{b,r}$ are the foward and backward rate coefficients of reaction r, that depends on the temperature T through the Ahrrenius Law:

$$k_{f,r} = A_r T^{\beta_r} e^{-\frac{E_{a,r}}{\mathcal{R}T}}; (2.4)$$

$$k_{b,r}(\phi) = \frac{k_{f,r}(\phi)}{\left(\frac{P^0}{\mathcal{R}T}\right)^{\sum_{n=1}^{N} \nu_{n,r}} e^{\left(\frac{\Delta S_r^0}{\mathcal{R}} - \frac{\Delta H_r^0}{\mathcal{R}T}\right)}},$$
(2.5)

in which \mathcal{R} is the universal gas constant, $P^0=1$ atm is the reference pressure, A_r represents the frequency factor, $E_{a,r}$ represents the activation energy, β_r is the temperature exponent, ΔS_r^0 is the entropy change, and ΔH_r^0 is the enthalpy change in the reference state of reaction r (POINSOT; VEYNANTE, 2005).

The elementary reactions present in combustion and respective Ahrrenius parameters (A, β, E_a) are usually given in the form of a detailed mechanism as input file in computational fluid dynamic codes, as an exemple the Gri 3.0 mechanism (SMITH *et al.*, 2000) containing 53 species and 325 reactions, very utilized in combustion numerical simulations for methane and natural gas fuels, represented in Fig. 2.1.

In the combustion process, a chain of elementary reaction produces radicals that further react and can produce more radicals, until a chain-terminating reaction produces stable species. As exemples, considering the reactions involved in the hydrogen oxidation, a chain initiation reaction is:

$$H_2 + M \rightleftharpoons H^* + H^* + M, \tag{2.6}$$

which produces H^* radicals through dissociation of H_2 . M is a third body that participates in the collision. A chain-branching reaction involves the consumption of a radical and formation of two radicals species:

$$O^* + H_2O \rightleftharpoons OH^* + OH^*, \tag{2.7}$$

and a chain-terminating reaction:

$$H^* + OH^* + M \rightleftharpoons H_2O + M, \tag{2.8}$$

that produces the stable species H₂O (TURNS, 1996).

```
! GRI-Mech Version 3.0 7/30/99 CHEMKIN-II format
! See README30 file at anonymous FTP site unix.sri.com, directory gri;
! WorldWideWeb home page http://www.me.berkeley.edu/gri_mech/ or
! through http://www.gri.org , under 'Basic Research',
! for additional information, contacts, and disclaimer
ELEMENTS
O H C N AR
END
SPECIES
                 0
                          02
                                   OH
                                            H20
                                                     H<sub>0</sub>2
                                                              H202
H<sub>2</sub>
        H
C
        CH
                 CH<sub>2</sub>
                          CH2(S)
                                   CH<sub>3</sub>
                                            CH4
                                                     CO
                                                              C<sub>0</sub>2
HCO
        CH20
                 CH20H
                          CH30
                                   CH30H
                                            C2H
                                                     C2H2
                                                              C2H3
                          HCCO
C2H4
        C2H5
                 C2H6
                                   CH2C0
                                            HCCOH
                                                              NH
                                                     N
NH<sub>2</sub>
        NH3
                 HNN
                          NO
                                   NO2
                                            N20
                                                     HNO
                                                              CN
HCN
        H<sub>2</sub>CN
                 HCNN
                          HCNO
                                   HOCN
                                            HNCO
                                                     NCO
                                                              N<sub>2</sub>
AR
        C3H7
                 C3H8
                          CH2CH0
                                   CH3CH0
END
! THERMO
! Insert GRI-Mech thermodynamics here or use in default file
! END
                                                \boldsymbol{A}
                                                              β
                                                                        Ea
REACTIONS
                                             1.200E+17
                                                           -1.000
                                                                           .00
20+M<=>02+M
H2/ 2.40/ H20/15.40/ CH4/ 2.00/ CO/ 1.75/ CO2/ 3.60/ C2H6/ 3.00/ AR/ .83/
0+H+M<=>OH+M
                                             5.000E+17
                                                           -1.000
                                                                          .00
H2/2.00/ H20/6.00/ CH4/2.00/ CO/1.50/ CO2/2.00/ C2H6/3.00/ AR/ .70/
                                                            2.700
                                                                      6260.00
0+H2<=>H+0H
                                             3.870E+04
0+H02<=>0H+02
                                             2.000E+13
                                                             .000
                                                                          .00
0+H202<=>0H+H02
                                             9.630E+06
                                                            2.000
                                                                      4000.00
0+CH<=>H+C0
                                             5.700E+13
                                                             .000
                                                                          .00
0+CH2<=>H+HC0
                                             8.000E+13
                                                             .000
                                                                          .00
                                             1.500E+13
0+CH2(S) <=>H2+C0
                                                             .000
                                                                          .00
0+CH2(S)<=>H+HCO
                                             1.500E+13
                                                             .000
                                                                          .00
0+CH3<=>H+CH20
                                             5.060E+13
                                                             .000
                                                                          .00
0+CH4<=>0H+CH3
                                             1.020E+09
                                                            1.500
                                                                      8600.00
                                             1.800E+10
                                                             .000
0+CO(+M) <=>CO2(+M)
                                                                      2385.00
                        .000
                                 3000.00/
   LOW/ 6.020E+14
H2/2.00/ O2/6.00/ H2O/6.00/ CH4/2.00/ CO/1.50/ CO2/3.50/ C2H6/3.00/ AR/ .50/
0+HCO<=>0H+CO
                                             3.000E+13
                                                             .000
                                                                          .00
0+HCO<=>H+CO2
                                                             .000
                                             3.000E+13
                                                                          .00
                                                                      3540.00
0+CH20<=>0H+HC0
                                             3.900E+13
                                                             .000
0+CH2OH<=>0H+CH20
                                             1.000E+13
                                                             .000
                                                                          .00
0+CH30<=>0H+CH20
                                             1.000E+13
                                                             .000
                                                                          .00
0+CH30H<=>0H+CH20H
                                             3.880E+05
                                                            2.500
                                                                      3100.00
0+CH30H<=>0H+CH30
                                             1.300E+05
                                                            2.500
                                                                      5000.00
                                                             .000
0+C2H<=>CH+C0
                                             5.000E+13
                                                                          .00
O+C2H2<=>H+HCCO
                                             1.350E+07
                                                            2.000
                                                                      1900.00
0+C2H2<=>0H+C2H
                                             4.600E+19
                                                           -1.410
                                                                     28950.00
0+C2H2<=>C0+CH2
                                             6.940E+06
                                                            2.000
                                                                      1900.00
0+C2H3<=>H+CH2C0
                                                             .000
                                             3.000E+13
                                                                          .00
0+C2H4<=>CH3+HC0
                                             1.250E+07
                                                            1.830
                                                                       220.00
0+C2H5<=>CH3+CH20
                                                             .000
                                             2.240E+13
                                                                          .00
0+C2H6<=>0H+C2H5
                                             8.980E+07
                                                            1.920
                                                                      5690.00
                                                                          .00
0+HCCO<=>H+2CO
                                             1.000E+14
                                                             .000
O+CH2CO<=>OH+HCCO
                                                             .000
                                                                      8000.00
                                             1.000E+13
0+CH2CO<=>CH2+CO2
                                             1.750E+12
                                                             .000
                                                                      1350.00
```

Figure 2.1 – GRI 3.0 detailed chemical kinetics mechanism. All reactions are available in SMITH *et al.* (2000).

2.2 Laminar premixed flame

Accurate numerical simulations of laminar flames are important as laminar flame speeds are widely used for chemical kinetics mechanism validation agaist experimental data, and laminar flames form the elementary building block in turbulent combustion models such as the flamelet theory of turbulent flames (POINSOT; VEYNANTE, 2005).

When fuel and oxidizer are in a homogeneous mixture before entering the combustion chamber, the combustion regime is called premixed. The equivalence ratio (ϕ) is the ratio between the fuel-oxidizer mass fractions in the tested condition and at the stoichiometric condition, defined as:

$$\phi = \frac{\left(\frac{Y_F}{Y_O}\right)}{\left(\frac{Y_F}{Y_O}\right)_{stq}} = \frac{Y_F \nu_O' W_O}{Y_O \nu_F' W_F},\tag{2.9}$$

where Y is the mass fraction, ν' is the stoichiometric coefficient, the subscript F refers to the fuel, O refers to the oxidizer, and stq refers to the stoichiometric conditions. Therefore, $\phi < 1$ for fuel-lean mixtures, related to the excess of oxidizer, $\phi = 1$ for stoichiometric mixtures, and $\phi > 1$ for fuel-rich mixtures with excess of fuel (POINSOT; VEYNANTE, 2005).

The differential equations for a laminar flame are given by the transport of mass:

$$\frac{\partial \left(\rho u\right)}{\partial x} = 0,\tag{2.10}$$

the transport of species:

$$\frac{\partial}{\partial x}(\rho(u+V_n)Y_n) = \dot{\omega}_n, \tag{2.11}$$

and the transport of energy:

$$\rho c_p u \frac{\partial T}{\partial x} = -\sum_{n=1}^N h_n \dot{\omega}_n + \frac{\partial}{\partial x} \left(\lambda \frac{\partial T}{\partial x} \right) - \frac{\partial T}{\partial x} \left(\rho \sum_{n=1}^N c_{p,n} Y_n V_n \right)$$
(2.12)

in which ρ is the density, u is the velocity is the x direction, μ the dynamic viscosity, λ is the thermal conductivity, p is the pressure, N is the total number of species, c_{pn} is the heat capacity at constant pressure, Y_n is the mass fraction, V_n is the diffusion velocity, h_n is the specific enthalpy of species n. From the reference frame of the flame, the unburned mixture mass flux is related to the flame propagation speed through $\dot{m}'' = \rho s_L$. For a laboratory flat flame,

the combustion is characterized by a deflagation wave, which is subsonic; as a consequence, the pressure gradients were neglect and the properties can be evaluated at the thermodynamic pressure P. Considering an ideal gas, the equation of state is given by:

$$\rho = \frac{P\bar{W}}{\mathcal{R}T},\tag{2.13}$$

in which \overline{W} is the mean molecular weight of the mixture and T is the temperature (POINSOT; VEYNANTE, 2005).

The thermodynamic properties are evaluated as a function of temperature through NASA-7 polynomials (KEE *et al.*, 2017):

$$\frac{c_p^{\circ}}{\mathcal{R}} = a_1 + a_2 T + a_3 T^2 + a_4 T^3 + a_5 T^4, \tag{2.14}$$

$$\frac{h^{\circ}}{\mathcal{R}T} = a_1 + \frac{a_2}{2}T + \frac{a_3}{3}T^2 + \frac{a_4}{4}T^3 + \frac{a_5}{5}T^4 + \frac{a_6}{T},\tag{2.15}$$

$$\frac{s^0}{\mathcal{R}} = a_1 \ln T + a_2 T + \frac{a_3}{2} T^2 + \frac{a_4}{3} T^3 + \frac{a_5}{4} T^4 + a_7. \tag{2.16}$$

As the flow is composed by a mixture of species, molecules diffuse from high to low concentration regions. Accurate modeling of the species diffusion is given through the multicomponent formulation. The computational cost of the multicomponent method arises from the inversion of a $N \times N$ matrix of binary diffusion coefficients (\mathcal{D}_{ni}) at each spatial and time step. As an alternative, accurate predictions can be obtained through the mixture-averaged formulation, that considers that the species diffuse into a mixture. The unity-Lewis assumption is given considering the thermal diffusivity equal to the mass diffusivity; the complete formulation can be found at POINSOT and VEYNANTE (2005).

The boundary conditions are given by zero-gradient $(\partial/\partial z)$ at the fresh reactants inlet and for the hot burnt gases. The initial conditions of unburned gas composition and temperature are set for the mixture. The laminar flame thickness (δ_L^0) can be obtained through:

$$\delta_L^0 = \frac{T_b - T_u}{max\left(\left|\frac{\partial T}{\partial x}\right|\right)},\tag{2.17}$$

in which T_b and T_u refer to the burned and unburned gas temperatures (POINSOT; VEYNANTE, 2005).

A typical flame structure can be observed in Fig. 2.2. The unburned gas region at the temperature T_u is called preheat zone, with small amount of heat released to the flow. The shaded area delimits the flame thickness defined in Eq. 2.17. In this region, called reaction zone, the fuel and the oxidizer are consumed and converted to products, while the reactions release heat resulting in a considerable rise in temperature, and characterized by a fast reaction rate. After the reaction zone, the post-flame zone is characterized by a slow reaction rate (TURNS, 1996).

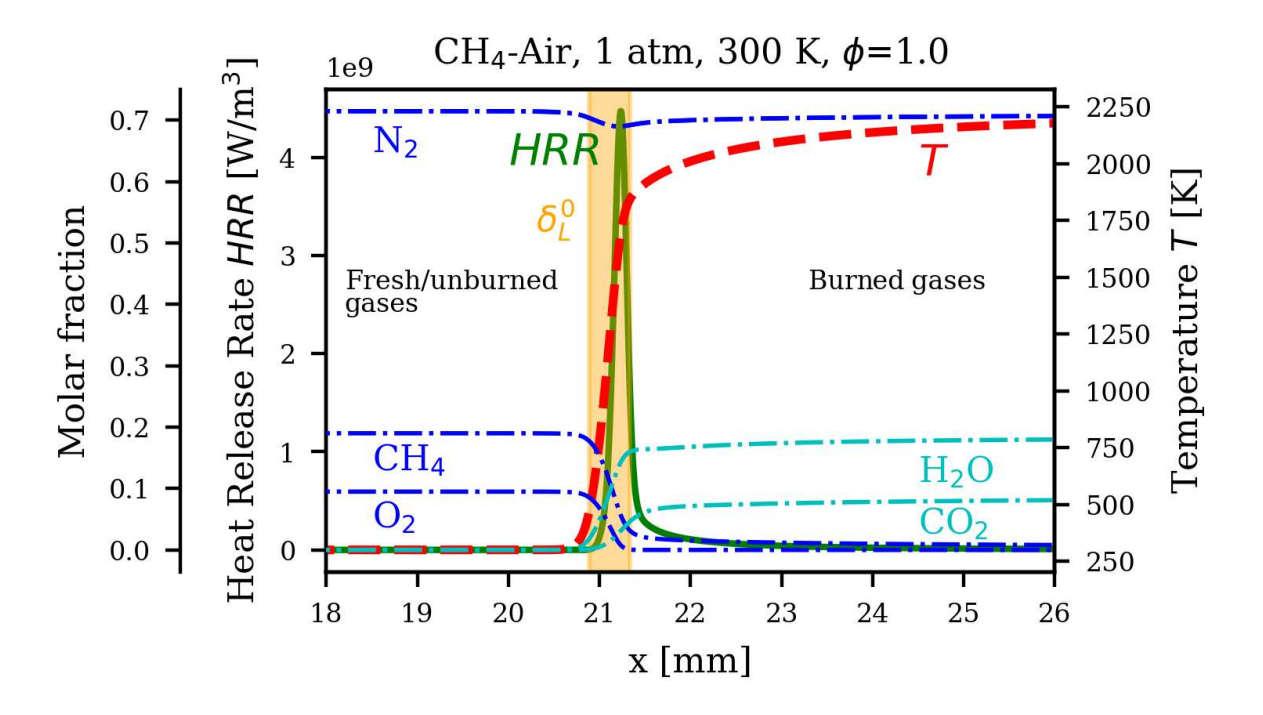


Figure 2.2 – Stoichiometric methane-air flame strucure at P=1 atm and $T_u=300$ K with the Gri 3.0 (SMITH *et al.*, 2000) chemical kinetics mechanism.

2.3 Ignition delay time

Ignition delay time is the time required for a mixture of fuel and oxidizer to react in a certain condition of pressure and temperature; the ignition point can be defined by the rise in temperature or species concentrations (Su *et al.*, 2024), such as the OH* radical in Fig. 2.3. Chemical kinetics mechanisms are validated with ignition delay time predictions against shock tube experiments (HONG *et al.*, 2011).

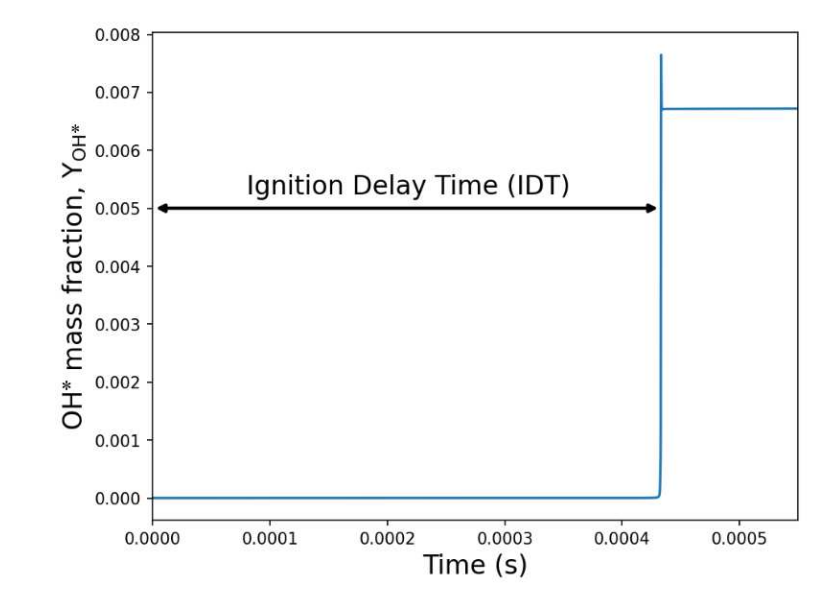


Figure 2.3 – Ignition delay time according to the OH* radical mass fraction. Source: Adapted from Goodwin *et al.* (2025).

Ignition delay time can be obtained through a batch reactor simulation at constant volume, associated with the mass conservation:

$$\frac{dm}{dt} = \sum_{in} \dot{m}_{in} - \sum_{out} \dot{m}_{out} + \dot{m}_{wall}, \qquad (2.18)$$

in which m is the mass, \dot{m}_{in} refers to the mass flow rate entering and \dot{m}_{out} the mass flow rate leaving the control volume, and \dot{m}_{wall} refers to the production on the surface. The species conservation gives:

$$\frac{d(mY_n)}{dt} = \sum_{in} \dot{m}_{in} Y_{n,in} - \sum_{out} \dot{m}_{out} Y_n + \dot{m}_{n,gen}, \tag{2.19}$$

in which \dot{m}_{qen} is the mass flow rate generated on the surface. From the energy equation:

$$\frac{dU}{dt} = \dot{Q} - p\frac{dV}{dt} + \sum_{in} \dot{m}_{in} h_{in} - h \sum_{out} \dot{m}_{out}.$$
 (2.20)

in which U is the internal energy and \dot{Q} is the heat added to the control volume (GOODWIN *et al.*, 2025).

2.4 Global chemical kinetics mechanisms

Detailed chemical schemes account for calculations of all reactions and intermediate species present in combustion. Due to the large number of species and reaction

steps, computational cost becomes an issue when coupling detailed chemical schemes with transport equations solvers for turbulent flows. Hopefully, with good agreement, optimized chemical schemes that reproduce the effects of detailed chemical kinetics allow for a computational cost reduction. Accurate simulations of combustion must take into account physical phenomena characterized by a wide range of spatial and time scales, as shown in Tab. 2.1. As turbulent direct numerical simulations (DNS) and Large Eddy Simulations (LES) solving the transport equations within those scales are often pohibitive, the detailed chemistry description that includes intermediate species formation and destruction can be modeled with good accuracy through the optimization of smaller mechanisms that are still representative for the major products such as CO_2 , H_2O , CO, nitrogen oxides (NO_x) , sulfur oxides (SO_x) , soot and unburned hydrocarbons (UHCs) (CAILLER, 2018).

Table 2.1 – Time and spatial scales associated with the physical phenomena present in combustion chambers.

Phenomenon	$\mathcal{O}(\text{spatial scales})$	O(time scales)
Combustion Chamber	0.1-1 m, Diameter	
Combustion Chamber	1-10 m, Length	-
Mean Flow	0.1 - 1 m	1 - 10 ms
Heat Transfer	0.01 - 10 mm	0.1 - 1 s
NO_x	_	0.1 s
Break-up of liquid fuel	1 mm	0.1 - 1 ms
into droplets		
Droplets Evaporation	0.01 mm	1 ms
Flame Thickness	< 1 mm	-
Acoustics	-	1 ms
Heat Release	-	0.1 ms
Radicals Formation or	-	10 μs
Destruction		
Turbulence	10 μm - 10 mm	1 - 10 μs

Source: Adapted from CAILLER (2018) and MIRA (2024).

A global chemical kinetics mechanism can be represented as:

$$F + aO \rightarrow bPr,$$
 (2.21)

in which F represents the fuel, O the oxidizer and Pr the products. The production rate is given by:

$$\dot{\omega} = k_f [F]^{n_F} [O]^{n_O},$$
 (2.22)

The exponents n_F and n_O relate to the reaction order. The reaction is in order of n_F with respect to the fuel, order n_O with respect to the oxidizer, and $n_F + n_O$ overall order. The foward reaction rate coefficient is given by the Ahrrenius law (TURNS, 1996):

$$k_f = AT^{\beta} e^{-\frac{E_{a,g}}{\mathcal{R}T}},\tag{2.23}$$

in which $E_{a,g}$ is the global chemical kinetics mechanism activation energy.

WESTBROOK and DRYER (1981) presented one of the first works on global chemical mechanisms that reproduce experimental laminar flame speeds. The authors found that the adjustment of the rate constants could provide a better prediction of laminar flame speeds for different mixtures regarding the computational issue of the coupling between detailed kinetics and complex fluid dynamics simulations. The one-step mechanism provided good predictions for flame speed; moreover, two-step mechanisms yield good estimation for the burned gas temperatures. These parameters resulted in good predictions for the studied hydrocarbons and the available data at that time, but new optimized mechanism valid for a variety of conditions, other quantities as temperature profiles, heat helease, pollutant concentrations, and based on updated experimental and detailed mechanisms data were required and are still being developed nowadays.

The work of PETERS *et al.* (1993) compiled the efforts in mechanisms systematically reduced (2-6 steps) through steady-state and partial-equilibrium approximations. The authors stated that steady-state approximations perform well for hydrocarbon fuels, as its combustion is characterized by low radical levels; whereas for hydrogen flames the formation of radicals leads to significant transient effects, with less accuracy of asymptotics descriptions. Analytical reduced mechanisms presented good predictions in recent works as the three-step mechanism developed by WEEKES *et al.* (2023) for Moderate or Intense Low-oxygen Dilution Conditions (MILD) of propane (C₃H₈) combustion.

FRANZELLI *et al.* (2010) showed that a two-step chemical scheme with the Arrhenius parameters fitted as functions of the equivalence ratio for kerosene fuel (molar fraction: 74% $C_{10}H_{22}$, 15% $C_{9}H_{12}$, and 11% $C_{9}H_{18}$) yields good estimates over a wide range of temperature, pressure, and diluent concentration; further, the methodology was applied to build a two-step mechanism for methane fuel and coupled to a LES of a lean partially premixed swirled flame gas turbine combustor, showing good agreement with experimental measurements for stable turbulent flows (FRANZELLI *et al.*, 2012). WESTBROOK and DRYER (1981) and

FRANZELLI *et al.* (2010) applied an analytical relation between the pressure coefficient and the fuel and oxidizer concentration exponents that holds potential to minimize computational costs by providing a set of rate parameters suitable for different pressure conditions.

Further, CAILLER et al. (2017) presented the virtual chemistry framework to build up an optimized mechanism for methane flames through virtual products. The optimization of the reaction rate parameters and thermodynamic NASA polynomial coefficients leads to virtual species to describe the target properties of the flow; in their study, the two-step mechanism was capable of predicting better temperature profiles than the one-step version. The study was further extended in the work of CAILLER et al. (2020), which presented good predictions for two-dimensional laminar partially-premixed burner relative to the respective detailed reference mechanism. A key aspect of their study was the use of a genetic algorithm to find the best parameters evaluated using a fitness function definition that accounts for the temperature profile and laminar flame speed outputs from a detailed mechanism.

Recently, KILDARE *et al.* (2024) fitted the Arrhenius parameters for hydrogen and methane fuels one-step mechanisms, providing functional forms of initial temperature, pressure, and oxygen mole fraction valid for Moderate and Intense Low Oxygen Dilution (MILD) conditions; The hydrogen mechanism was capable of capturing temperature and heat release profiles for CFD turbulent simulations with, approximately, a 100 times computational cost reduction compared to the detailed description. Another noteworthy study was the one-step hydrogen mechanism presented by MILLÁN-MERINO and BOIVIN (2024), which in 2025 ranks among the six most downloaded articles in the prestigious Combustion and Flame journal, highlighting the significance of recent advancements in optimized global mechanisms.

2.5 Supercritical combustion

When the fluid is at pressure and temperature conditions above the critical point, it is neither in the gas phase nor the liquid phase, but in the supercritical state, as shown in the phase diagram in Fig. 2.4. The critical pressure (P_c) and temperature (T_c) of the stable chemical species present in this dissertation are given in Tab. 2.2. The transcritical state occurs when only the pressure or the temperature is above the critical value. Combustion modeling involves solving the transport equations plus a relation between density and pressure through an equation of state (EoS), often employing the ideal-gas (IG) EoS. However, in the supercritical/transcritical state, the utilization of the real-fluid equations has shown significant

effects in predicting quantities that characterize the combustion phenomena, such as laminar flame speed (LFS), ignition delay time (IDT), and flame structure.

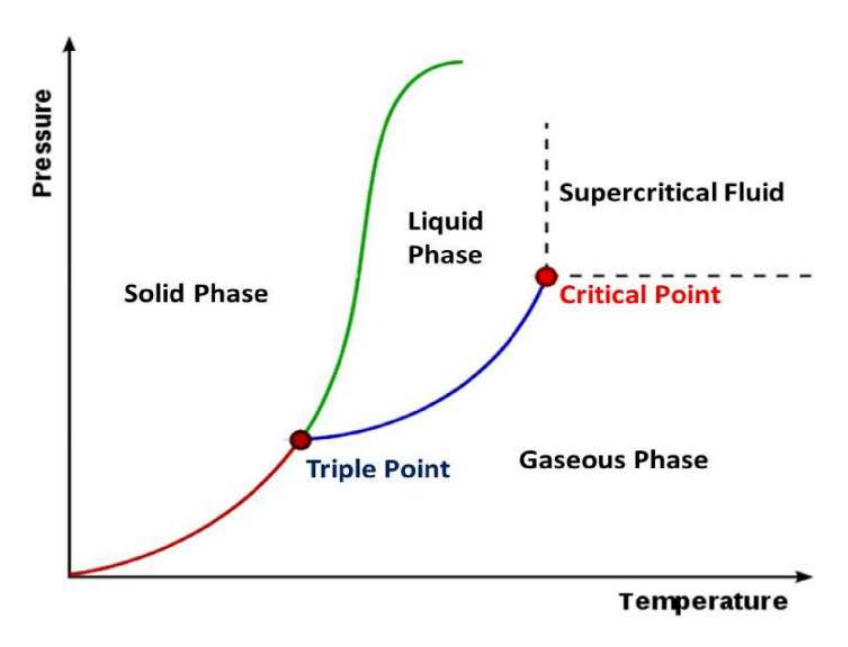


Figure 2.4 – Phase diagram. Source: Gupta et al. (2014).

Table 2.2 – Critical properties.

Species	P_c [atm]	T_c [K]
C_2H_5OH	61	515
H_2	13	33
O_2	50	155
N_2	34	126
CO_2	73	304
H_2O	218	647

Source: Data from NATIONAL INSTITUTE OF STANDARDS AND TECHNOLOGY (2023).

ZHANG et al. (2024) studied supercritical CO_2 diluted in oxy-syngas and oxy-methane flames under 700-800 K and 100-300 atm; they found that the real-fluid effects can increase or decrease the laminar flame speeds depending on the unburned/fresh gas temperature $(T_u \text{ or } T_f)$. LV et al. (2025) studied laminar hydrogen premixed flames of at ultra-high pressure and cryogenic conditions $(T_f = 50\text{-}350 \text{ K} \text{ and } 100\text{-}400 \text{ atm})$, and showed that the real gas equation of state was important to predict flame structure in the fresh gas region and for laminar flame speeds. BAI et al. (2025) found the the real fluid effects can reach 35% in laminar flame speeds at 100 atm in hydrogen-oxygen flames diluted by H_2O , that has a high polarization. They also found that the real-fluid effects results in 8% discrepancy for laminar flames of dimethyl

ether (DME) and n-heptane at 20-25 atm. PLÁCIDO *et al.* (2024) studied real-fluid effects in mixtures of ethanol, gasoline and diesel surrogates, finding approximately 20% discrepancy from ideal gas assumption in predicting ignition delay times at 150 atm.

Real-fluid effects can be analyzed through the Peng-Robinson (PR) equation of state:

$$P = \frac{\mathcal{R}T}{V - b} - \frac{\alpha(T)}{V(V + b) + b(V - b)}$$

$$\tag{2.24}$$

in which P is the pressure, \mathcal{R} is the universal gas constant, T is the temperature, and V is the volume. The parameter b is the Van der Waals repulsive volume correction, and α is the attraction parameter, given by:

$$b = 0.07780 \frac{\mathcal{R}T_c}{P_c},\tag{2.25}$$

$$\alpha = \left(1 + \kappa \left(1 - \sqrt{T/T_c}\right)\right)^2 0.45724 \frac{\mathcal{R}^2 T_c^2}{P_c},\tag{2.26}$$

in which κ is given in function of the acentric factor (ω):

$$\kappa = 0.37464 + 1.54226\omega - 0.26992\omega^2. \tag{2.27}$$

The critical property values (P_c , T_c) are documented in the literature for stable species such as H_2 and O_2 , derived from experimental data. However, the properties of some species must be estimated, as these values are unavailable for many intermediate and radical species. The Joback group contribution method (JOBACK, 2005) was utilized in the work of PLÁCIDO *et al.* (2024); PLÁCIDO (2024) to obtain the critical parameters for these species.

3 ETHANOL

This chapter presents new two-step chemical mechanisms for ethanol-air laminar premixed flames, that comprises the reaction of fuel oxidation into carbon monoxide (CO) and and water (H_2O) and the the CO - CO_2 equilibrium, thereby tracking the emission of carbon pollutants.

3.1 Methods

To calibrate the two-step mechanism, a recent reduced ethanol mechanism was utilized, comprised of 51 species and 627 reactions, developed and described in the study of gasoline/ethanol high-pressure combustion of PLÁCIDO *et al.* (2024), which is a reduced version based in the C1-C3 mechanism CRECK_2003_C1_C3_HT (RANZI *et al.*, 2014; RANZI *et al.*, 2015; BAGHERI *et al.*, 2020), validated for flame properties in the literature. The calibration conditions were set to 1 atm, 428 K, and $\phi = 0.6$ to $\phi = 1.8$. Those limits were set according to the available experimental data.

The flame simulations were carried through Cantera 3.0 (GOODWIN et al., 2023) open-source code which solves the transport equations for a freely propagating premixed laminar flame. The mixture-averaged transport model was adopted for the detailed mechanism due to its accuracy and moderate computational cost, and results in good predictions of experimental data for the studied conditions. For the two-step mechanisms, the unity-Lewis Number approximation was adopted, often present in optimization works as in WESTBROOK and DRYER (1981), FRANZELLI et al. (2010) and CAILLER et al. (2017).

The two-step chemical mechanism can be expressed as:

$$C_2H_5OH + 2O_2 \rightarrow 2CO + 3H_2O,$$
 (3.1)

$$CO + 0.5O_2 \rightleftharpoons CO_2, \tag{3.2}$$

with Arrhenius reaction rates coefficients:

$$k_{f,1}(\phi) = c_1(\phi) A_1 e^{-\frac{g_1(\phi)E_{a,g,1}}{\mathcal{R}T}},$$
(3.3)

$$k_{f,2}(\phi) = c_2(\phi) A_2 e^{-\frac{g_2(\phi)E_{a,g,2}}{\mathcal{R}T}},$$
 (3.4)

$$k_{b,2}(\phi) = \frac{k_{f,2}(\phi)}{\left(\frac{P^0}{RT}\right)^{\sum_{n=1}^{N} \nu_{n,2}} e^{\left(\frac{\Delta S_2^0}{R} - \frac{\Delta H_2^0}{RT}\right)}},$$
(3.5)

associated with the production rates:

$$\dot{\omega}_1(\phi) = k_{f,1}(\phi) [X_{C_2H_5OH}]^{n_F(\phi)} [X_{O_2}]^{n_O(\phi)}, \tag{3.6}$$

$$\dot{\omega}_2(\phi) = k_{f,2}(\phi)[X_{\text{CO}}][X_{\text{O}_2}] - k_{b,2}(\phi)[X_{\text{CO}_2}],\tag{3.7}$$

in which the correction functions $c(\phi)$ and $g(\phi)$ were introduced for the optimization process of the pre-exponetial factor and the global activation energy, respectively, and $n_F(\phi)$, $n_O(\phi)$ are the fuel (F) and oxidizer (O) reaction orders, also optimized.

The optimization was carried out using a Monte Carlo method, which generates independent random values for the optimization parameters. This method addresses minimization problems with numerous local minimums (KROESE; Rubinstein, 2012). Python version 3.11 produced uniformly distributed values within the optimization range using its module named random (PYTHON SOFTWARE FOUNDATION, 2024). The best parameter combination is selected based on the objective/fitness function value, which considers the relative difference (ε) between the global and the detailed (dtl) reference mechanisms:

$$\varepsilon_{s_L} = \frac{|s_{L,dtl} - s_L|}{s_{L,dtl}},\tag{3.8}$$

$$\varepsilon_{T} = \frac{||T_{dtl}(x_{dtl}) - T(x_{dtl})||}{||T_{dtl}(x_{dtl})||};$$
(3.9)

The fitness function (f) definition, similar to CAILLER et al. (2017), is given by:

$$f = w\varepsilon_{s_L} + (1 - w)\varepsilon_T, \tag{3.10}$$

in which w is the weight value for the laminar flame speed relative difference. Optimizing the temperature profile was more computationally expensive, so the value of w=0.1 was set, which corresponds to a 90% weight for the temperature profile. The best solution is given by the parameters associated with the minimum fitness value.

FRANZELLI *et al.* (2010) obtained a two-step mechanism that provided good predictions for kerosene laminar flame speed at different pressure conditions; this was achieved by imposing the following constraint - derived from an analytical relation between the pressure exponent (α_P) and the fuel and oxidizer reaction orders (n_F , n_O). From asymptotic analysis, MITANI (1980) presented an expression for the laminar flame speed depedence with pressure, which led to:

$$\alpha_P = \frac{n_F + n_O - 2}{2}. (3.11)$$

An estimate for the pressure exponent can be obtained from experimental or detailed chemical kinetics simulation data: $s_L(P,T)$ and $s_L^0(P^0,T^0)$, through the polynomial function (FRANZELLI *et al.*, 2010):

$$s_L(P,T) = s_L^0(P^0, T^0) \left(\frac{P}{P^0}\right)^{\alpha_P} \left(\frac{T}{T^0}\right)^{\alpha_T},$$
 (3.12)

for $T^0 = T$ and manipulating Eq. 3.12:

$$\alpha_P = \frac{ln(s_L) - ln(s_L^0)}{ln(P) - ln(P^0)},\tag{3.13}$$

these relations were imposed to obtain a global mechanism for ethanol-air premixed flames valid under 1-2 atm pressure conditions, following the procedure presented in the flowchart of Fig. 3.1.

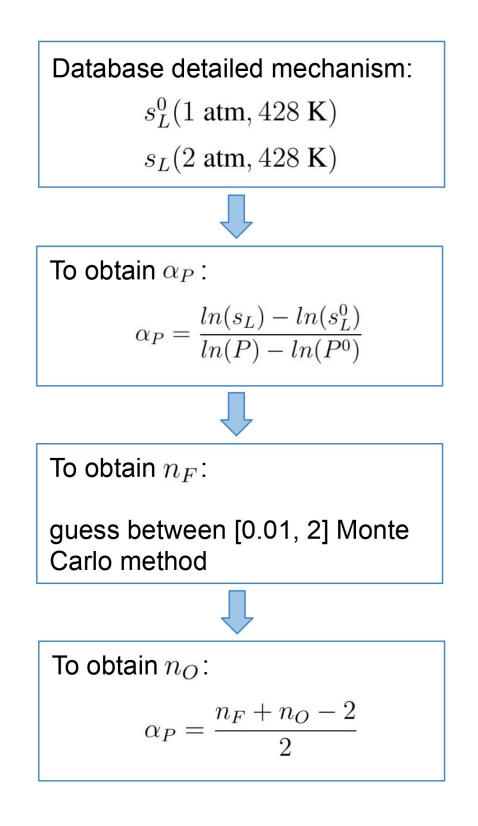


Figure 3.1 – Flowchart to obtain reaction orders for the two-step ethanol chemical kinetics mechanism.

3.2 Results

Figure 3.2 presents the relative differences and fitness function evolution according to the number of tested set of parameters $(c_1, c_2, g_1, g_2, n_F, n_O)$, called samples, which corresponds to three Monte Carlo simulation runs. Despite the variations in the relative difference profiles $(\varepsilon_{S_L}, \varepsilon_T)$ between the runs, due to the randomness of the optimization technique, the fitness function profiles (f) consistently show a decay as the number of samples increase. This indicates convergence towards the minimum of the f function, which is the main goal of the optimization.

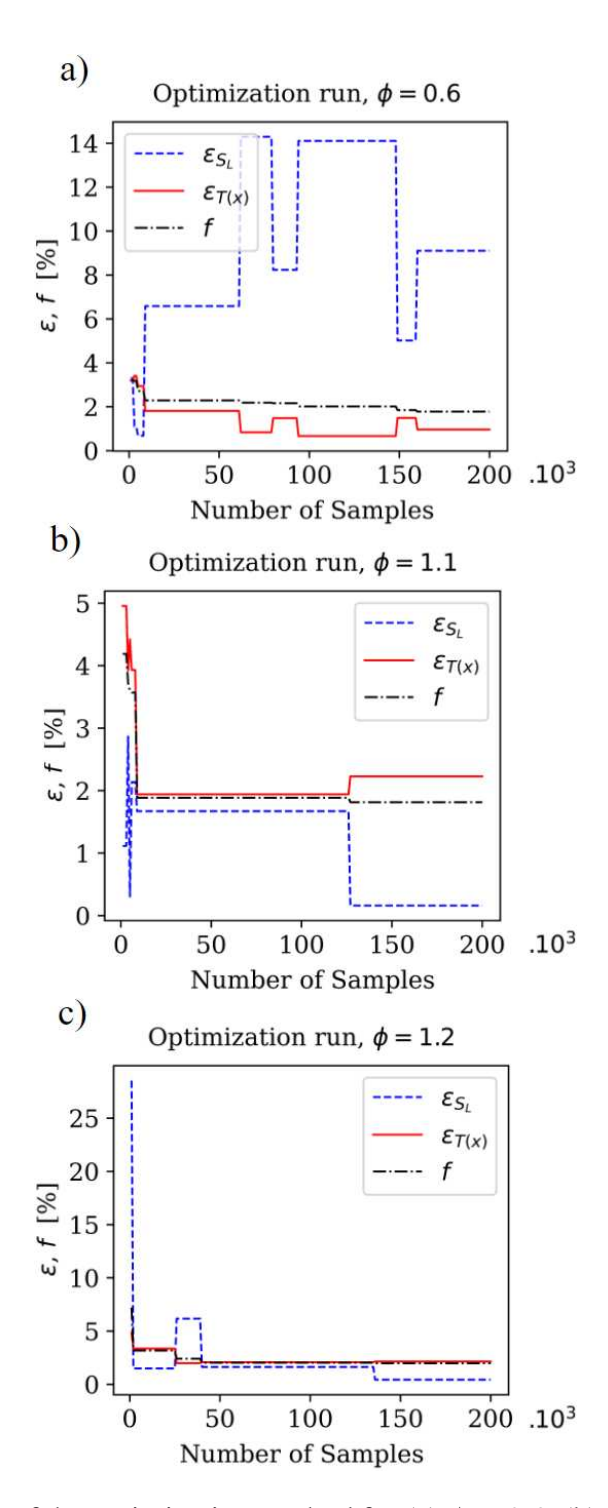


Figure 3.2 – Three runs of the optimization method for (a) $\phi = 0.6$, (b) $\phi = 1.1$ and (c) $\phi = 1.2$.

The obtained parameters of the two-step ethanol chemical kinetics mechanism at 1 atm are available in Tab. 3.1; laminar flame speeds (LFS) are available in Fig. 3.3, and temperature profiles are available in Fig. 3.4 and Fig. 3.5. The global mechanisms closely reproduce the flame speeds obtained from both the detailed mechanism and experimental data across a wide range of equivalence ratios. The deviation remains within $\pm 5\%$ for most

equivalence ratios, indicating a good predictive capability. At lean ($\phi=0.6$) and rich ($\phi=1.8$) limits, the deviation increases up to 10%. For $\phi=0.6$, despite the 10% overprediction in flame speed, the temperature profile remains in close agreement with the detailed model, with deviation below 3%. For rich mixtures, the global model slightly overpredicts peak temperatures ($\approx 6\%$). This discrepancy is attributed to the absence of intermediate and radical species in the global scheme, which in the detailed mechanism presents a endothermic behavior that lowers the flame temperature.

Table 3.1 – Two-step ethanol chemical kinetics mechanism parameters for P=1 atm, $\phi=0.6$ to $\phi=1.8$.

ϕ	c_1	c_2	n_F	n_O	g_1	g_2
0.6	47.875	0.043	0.155	1.964	0.809	0.747
0.7	17.280	0.100	0.346	1.548	0.901	0.941
0.8	78.011	0.031	0.406	1.406	1.082	0.666
0.9	95.603	0.731	0.309	1.464	1.087	1.718
1.0	16.593	0.091	0.357	1.274	1.106	1.141
1.1	33.905	0.058	0.262	1.581	0.918	0.945
1.2	17.983	0.347	0.235	1.731	0.696	1.568
1.3	50.860	0.067	0.397	1.458	0.931	1.382
1.4	99.937	0.985	0.369	1.581	0.892	2.224
1.5	18.205	0.250	0.546	1.245	0.979	8.362
1.6	37.634	2.758	0.240	1.724	0.901	6.121
1.7	34.019	4.494	1.767	0.298	0.762	8.913
1.8	22.738	8.941	1.591	0.572	0.665	3.784

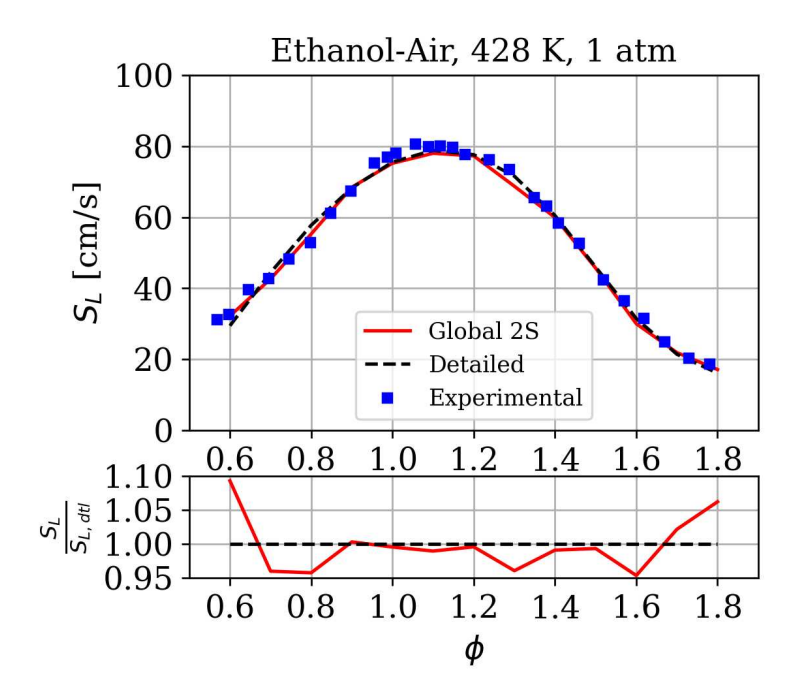


Figure 3.3 – Ethanol-air premixed laminar flame speed at P=1 atm and $T_u=428$ K.

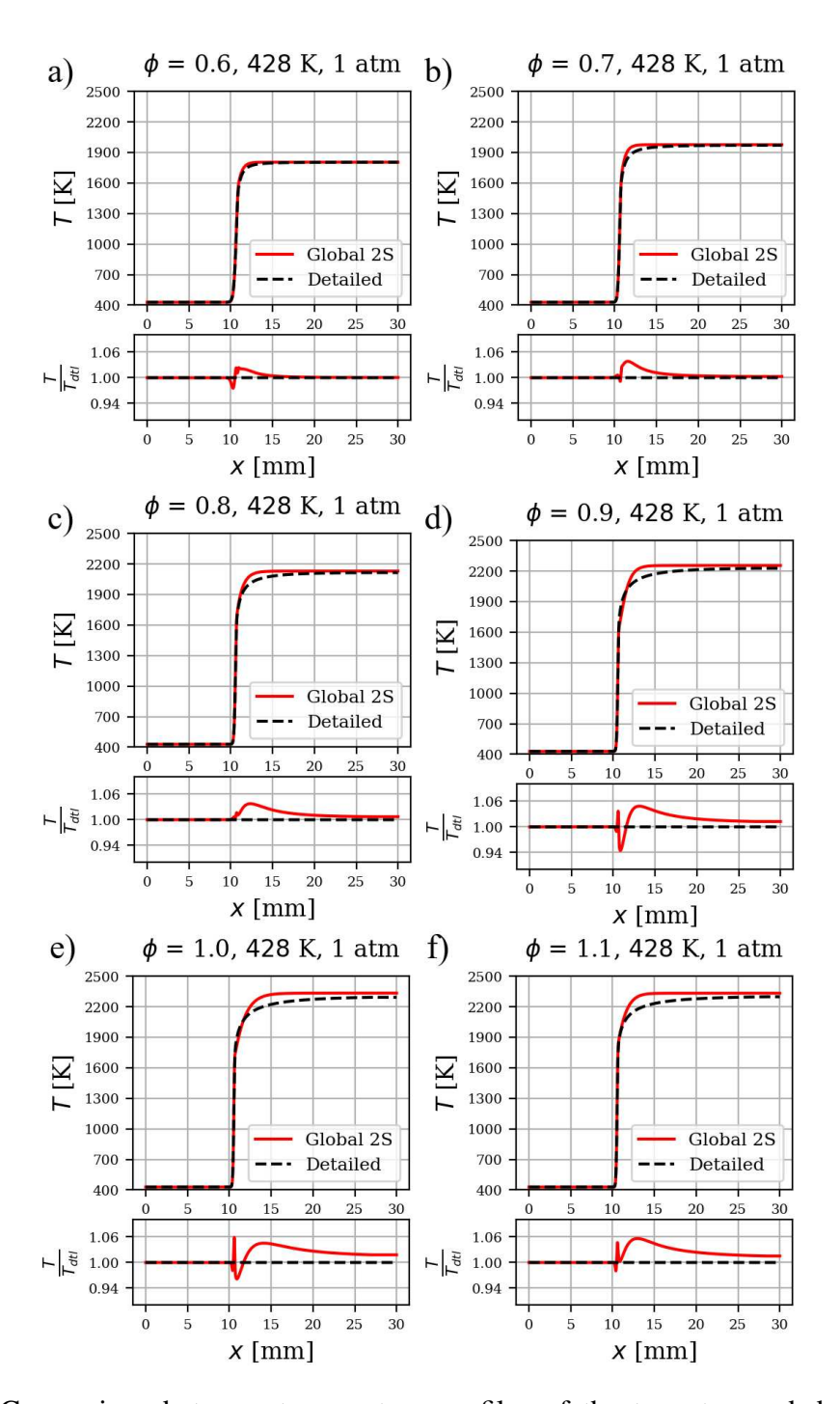


Figure 3.4 – Comparison between temperature profiles of the two-step and detailed ethanol chemical kinetics mechanisms for $\phi=0.6$ to 1.1 at P=1 atm and $T_u=428$ K.

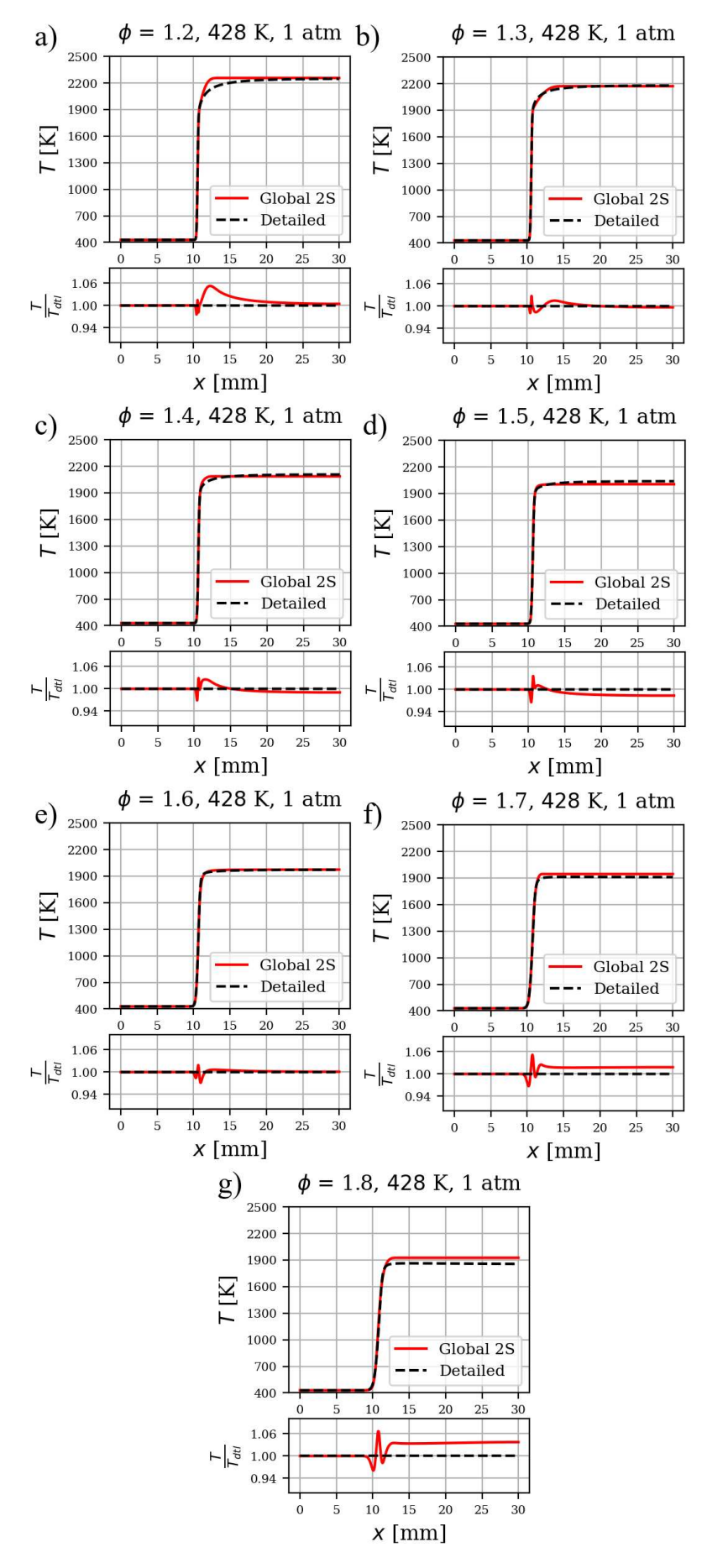


Figure 3.5 – Comparison between temperature profiles of the two-step and detailed ethanol chemical kinetics mechanisms for $\phi=1.2$ to 1.8 at P=1 atm and $T_u=428$ K.

ZHENG et al. (2024) presents shock tube measurements of stoichiometric laminar premixed ethanol flame speeds at atmospheric pressure and various initial temperatures, which align with previous experimental data documented by EISAZADEH-FAR et al. (2011), RAU et al. (2015), LIAO et al. (2007), and KATOCH et al. (2018). In Figure 3.6, the predictions for laminar flame speed and the experimental data are presented; even though the two-step mechanism was optimized for 428 K, it still maintains good agreement across the range of unburned gas temperature $300 \le T_u \le 500$ K, and overestimates the laminar flame speed for higher temperatures, showing limitations in capturing the temperature dependence of reaction rates at higher temperatures.

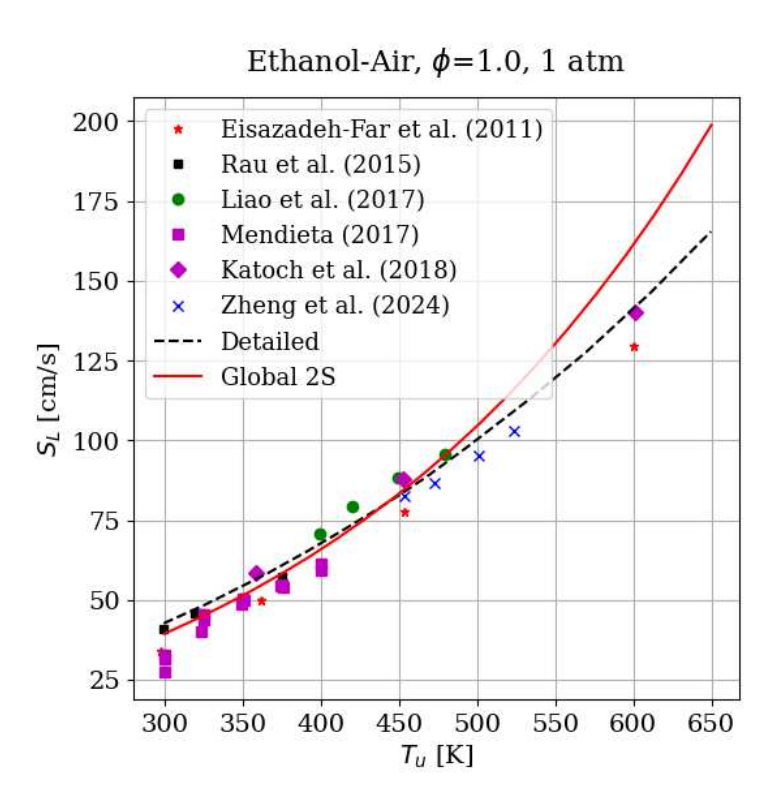


Figure 3.6 – Laminar flame speed comparison for different unburned gas temperatures between chemical kinetics mechanisms (lines) and experimental data (markers), for stoichiometric mixtures and P=1 atm.

For kerosene fuel, FRANZELLI et al. (2010) found an average pressure coefficient (α_P) over the pressure range of 1-12 atm (Fig. 3.7-a); however, for ethanol fuel, the pressure coefficient considerably varies, as shown in Fig. 3.7-b. In this work, the aimed laminar flame dependence between the reference pressure $P_0 = 1$ atm and P = 2 atm resulted in the values presented in Tab. 3.2, obtained with the analytical constraint of Eq. 3.13.

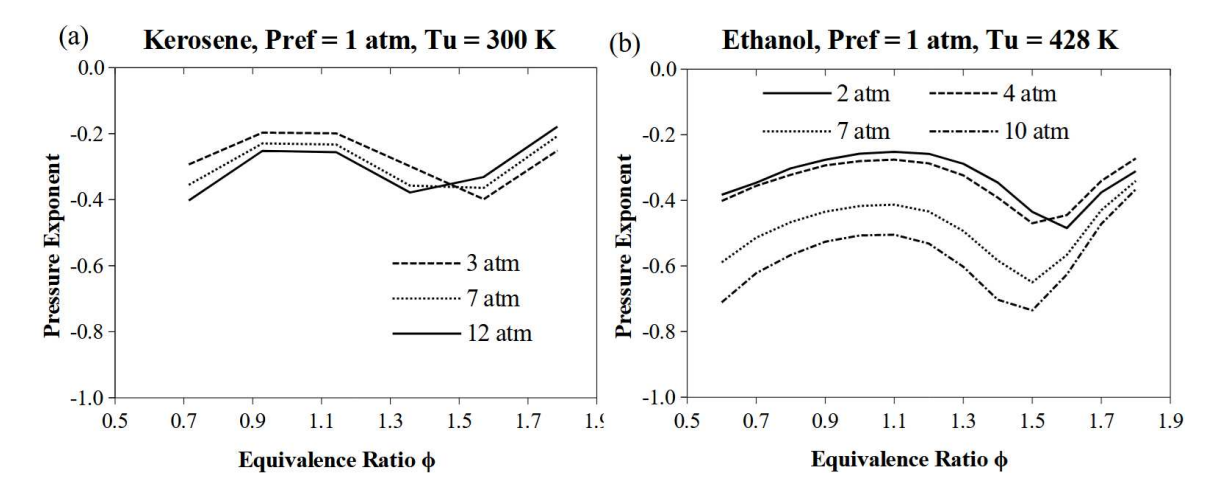


Figure 3.7 – Pressure exponent for the reference pressure of 1 atm, for (a) kerosene fuel, P=2 to 12 atm, $T_u=300$ K, and detailed chemical kinetics mechanism of LUCHE (2003), and (b) ethanol fuel, P=2 to 10 atm, $T_u=428$ K, detailed mechanism of PLÁCIDO *et al.* (2024).

Table 3.2 – Reactant order obtained through Equation 3.13 and the detailed mechanism of PLÁCIDO et al. (2024) for $T_u = 428 \text{ K}$, $P^0 = 1 \text{ atm}$, and P = 2 atm.

ϕ	$n_F + n_O$
0.6	1.234
0.7	1.308
0.8	1.395
0.9	1.448
1.0	1.484
1.1	1.496
1.2	1.484
1.3	1.423
1.4	1.308
1.5	1.130
1.6	1.031
1.7	1.248
1.8	1.378

The following results are related to the obtained parameters for 1-2 atm optimization, available in Tab. 3.3. Considering that Set 1 refers to the chemical kinetics mechanism optimized at 1 atm and Set 2 to the mechanism optimized for 1-2 atm with the analytical constraint, the laminar flame speeds (LFS) are represented in Fig. 3.8. Set 2 shows higher discrepancies for the lean and rich mixtures compared to Set 1 at 1 atm; however, it shows considerable better agreement for LFS at 2 atm. Set 1 LFS for rich mixtures are considerably overpredicted for 2 atm; this is associated with the higher order values, as shown by the red lines in Fig. 3.9. The Set 2 mechanism resulted in higher discrepancies in predict the temperature

profiles in Fig. 3.10 and Fig. 3.11 than Set 1 in Fig. 3.4 and Fig. 3.5, mainly at the rich limit for $\phi = 1.8$.

Table 3.3 – Optimized two-step ethanol mechanism parameters for P=1 and 2 atm, $\phi=0.6$ to $\phi=1.8$.

ϕ	c_1	c_2	n_F	n_O	g_1	g_2
0.6	0.341	8.326	1.018	0.212	1.027	2.351
0.7	0.186	9.069	1.191	0.119	0.992	2.086
0.8	23.024	4.965	1.209	0.191	1.258	2.079
0.9	21.075	0.644	1.256	0.194	1.187	1.569
1.0	62.689	0.023	1.225	0.255	1.323	0.581
1.1	29.708	0.261	1.169	0.331	1.204	1.513
1.2	4.003	3.559	1.089	0.391	1.085	2.371
1.3	1.342	2.210	1.229	0.191	1.101	2.324
1.4	0.085	6.456	1.064	0.246	1.065	3.012
1.5	11.868	2.559	0.182	0.948	2.216	1.833
1.6	97.185	22.685	0.139	0.891	2.967	1.721
1.7	65.310	32.573	0.893	0.357	2.652	2.008
1.8	0.333	6.006	0.882	0.498	1.673	2.001

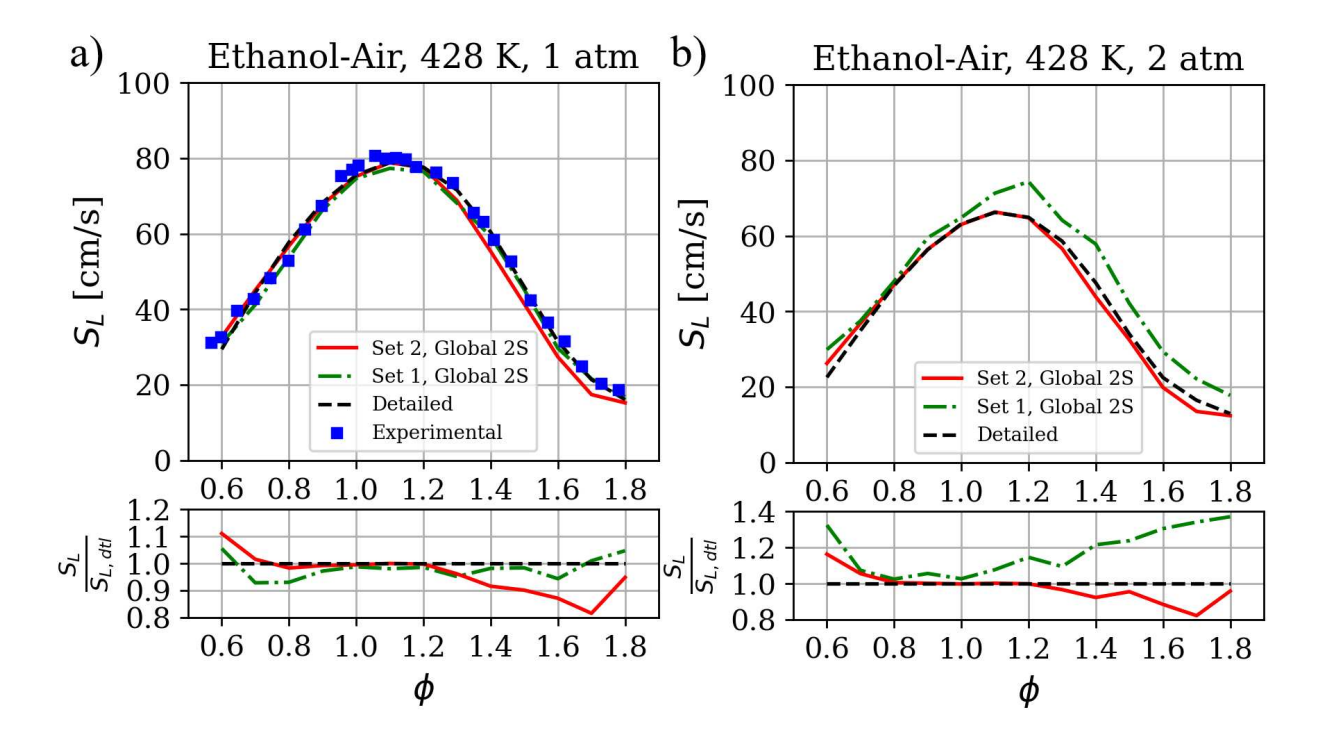


Figure 3.8 – Laminar flame speed for $T_u=428~{\rm K}$, (a) P=1 atm and (b) P=2 atm, according to the equivalence ratio.

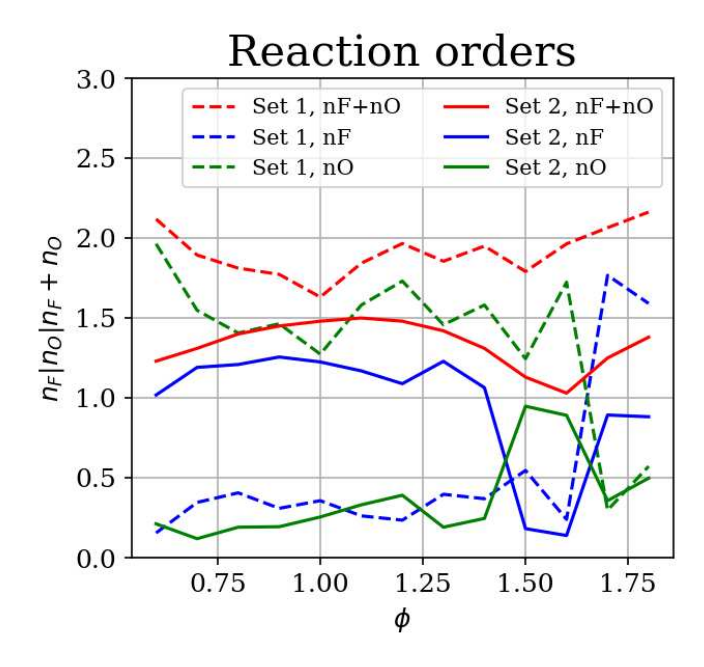


Figure 3.9 – Reaction orders for the two optimized sets of parameters according to the equivalence ratio.

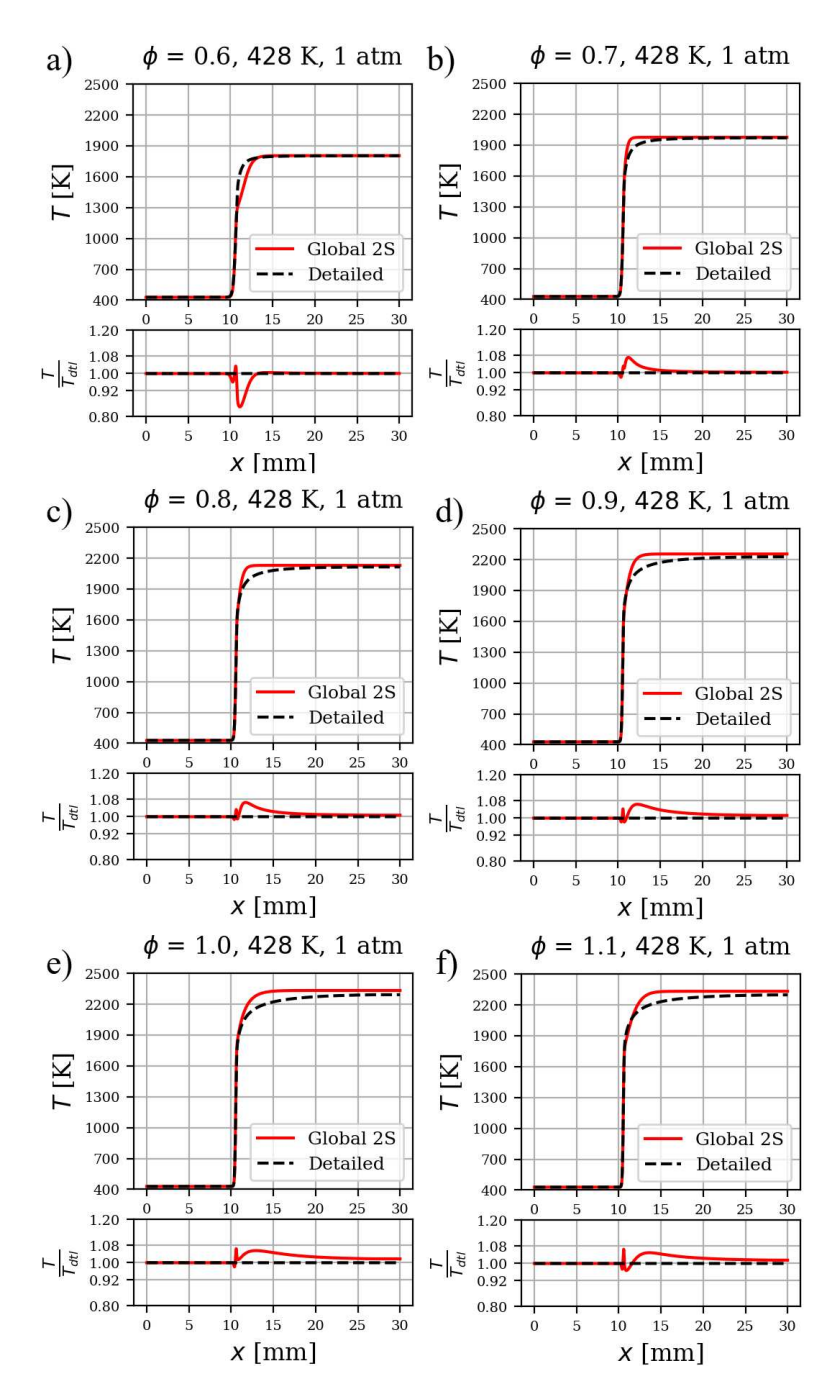


Figure 3.10 – Comparison between temperature profiles of the two-step mechanism optimized for P=1 and 2 atm and detailed ethanol chemical kinetics mechanisms, for $\phi=0.6$ to 1.1 at P=1 atm and $T_u=428$ K.

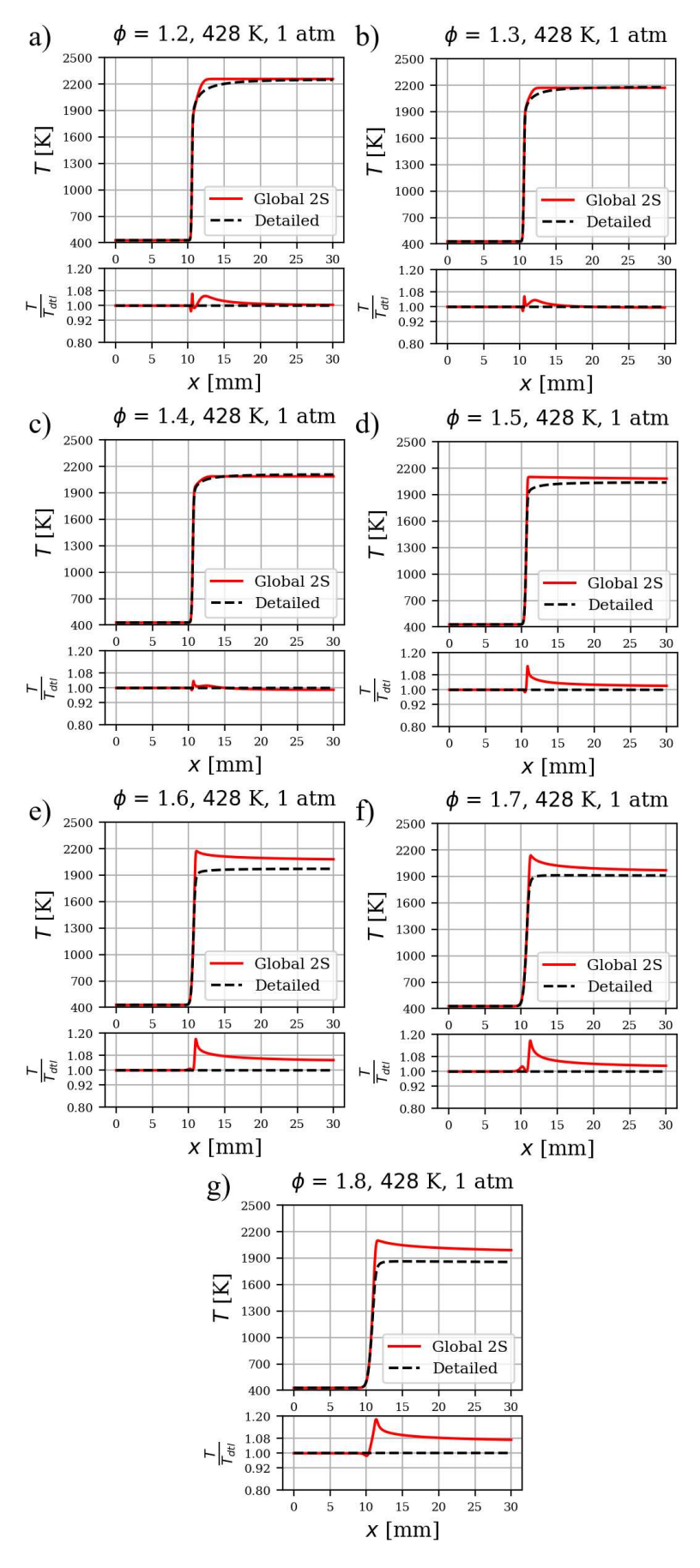


Figure 3.11 – Comparison between temperature profiles of the two-step mechanism optimized for P=1 and 2 atm and detailed ethanol chemical kinetics mechanisms for $\phi=1.2$ to 1.8 at P=1 atm and $T_u=428$ K.

The optimization of the global two-step ethanol mechanism successfully reproduced laminar flame speeds and temperature profiles with reasonable accuracy across a wide range of conditions, while discrepancies remain, particularly at the lean and rich limits. Overall, the results demonstrate that the proposed optimization framework can generate reduced chemical kinetics schemes capable of reproducing key combustion properties with satisfactory accuracy.

4 HYDROGEN

This chapter investigates the kinetics of laminar hydrogen flames. In Section 4.1, numerical simulations are conducted to analyze key combustion characteristics, such as flame speed, ignition delay time, flame structure, and the comparison of different chemical kinetics mechanisms under high-pressure. A sensitivity analysis is performed to identify the most relevant reactions and species in modeling high-pressure combustion. In Section 4.2, global mechanisms for ultra-high pressure premixed hydrogen-air flames are proposed, using the real gas Peng-Robinson equation of state.

4.1 Kinetics of high-pressure hydrogen flames

4.1.1 Methods

Three detailed hydrogen chemical kinetics mechanisms were employed for comparison: Li *et al.* (2004), Burke *et al.* (2012), and Konnov (2019). Those mechanisms were chosen because they have up to 15 species, as described in Tab. 4.1, making flame computations possible with a moderate computational cost; for high-pressure conditions, the flame thickness becomes more thin and more grid points are required, raising considerably the computational cost of solving the transport equations for each species at each grid point.

Table 4.1 – Detailed chemical kinetics mechanisms utilized in this dissertation.

Mechanism	Species	Reactions
Li et al. (2004)	13	25
Burke et al. (2012)	13	27
Konnov (2019)	15	75

4.1.2 Results

Figure 4.1 presents laminar flame speeds for H_2 -Air laminar premixed flames for $1 \le P \le 100$ atm. The H_2 -Air flames show a monotonic decrease in LFS with pressure; this behavior is reported experimentally in the work of Lu *et al.* (2020) for H_2/O_2 /diluent (N_2 , He, Ar, and CO_2) mixtures, for pressures up to 4 atm; the authors associated this behavior with the reduction of the radical pool with the increase of pressure. The reduction of the H^* , O^* , OH^* radical pool with increase of pressure is presented in Fig. 4.2 for stoichiometric H_2 -air mixture,

in which the red line represents the molar concentration of the species in the burned gases and the blue line the maximum molar concentration through the flame.

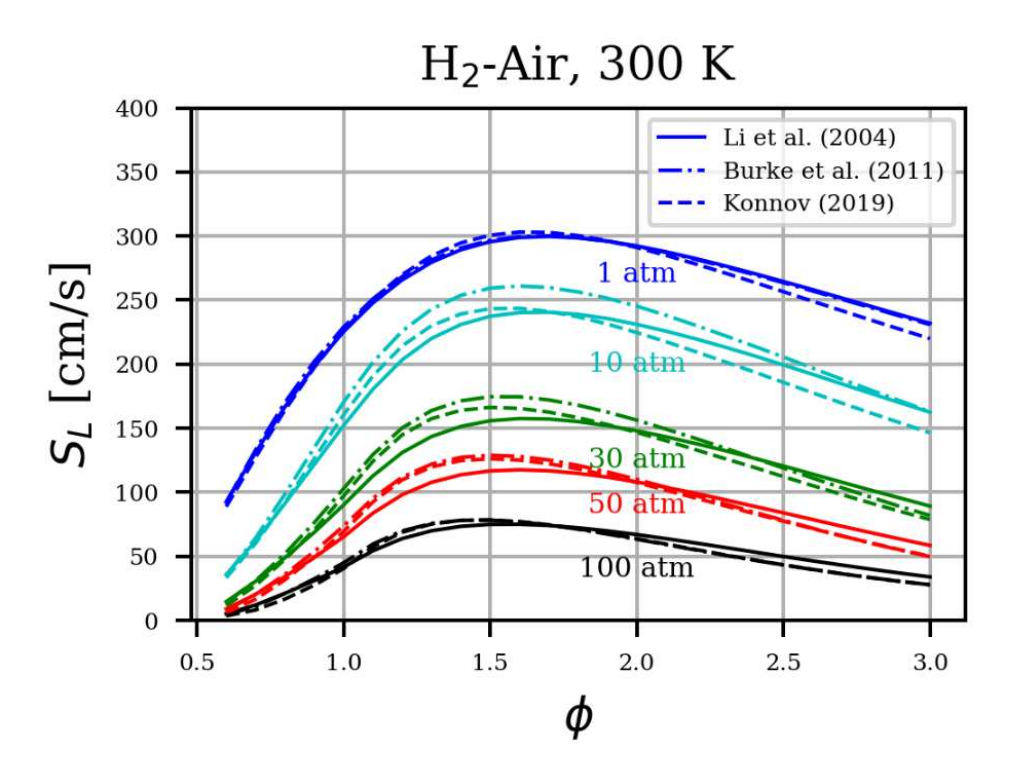


Figure 4.1 – Laminar flame speeds for hydrogen-air premixed flames at $T_u = 300$ K and P = 1 to 100 atm.

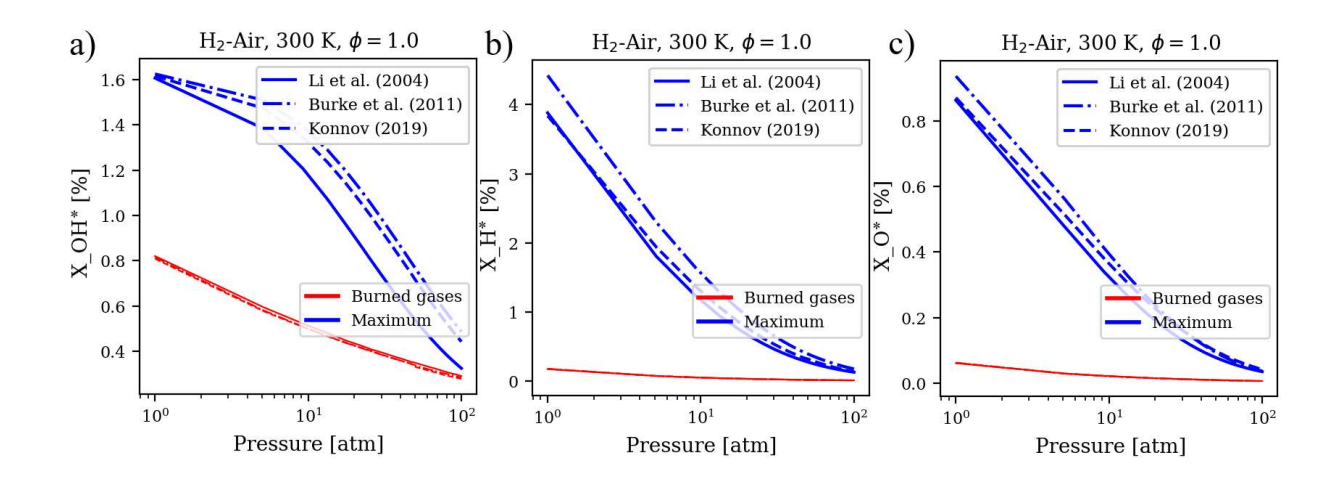


Figure 4.2 – OH* (a), H* (b), and O* (c) species profiles for H₂-air laminar preximed flames at $T_u = 300$ K and P = 1 to 100 atm.

Figure 4.3 shows that H_2O_2 and HO_2^* maximum molar fractions increases with pressure for H_2 -air stoichiometric mixture. For HO_2^* , the curve present a peak in 30 atm and then slightly decreases for 30-100 atm, which is related to the sensitivity coefficients of the

reaction $H^* + O_2$ (+M) \rightleftharpoons HO_2^* (+M) showed in the black line of Fig. 4.4 involving this species. A positive sensitivity coefficient means that the reaction affects laminar flame speeds in order to increase it, and negative sensitivity coefficient reduces LFS (Ronan *et al.*, 2022). Higher sensitivity values in module indicates the importance of the reaction in the LFS results. The most relevant reactions: $H^* + O_2 \rightleftharpoons O^* + OH^*$, $H_2 + OH^* \rightleftharpoons H^* + H_2O$, include three radical species (H*, O*, OH*) and the major product H_2O . It also shows that the reaction $H^* + O_2$ (+M) $\rightleftharpoons HO_2^*$ (+M), including the HO_2^* radical, becomes more relevant with the increase of pressure, reducing the LFS with negative sensitivity coefficient.

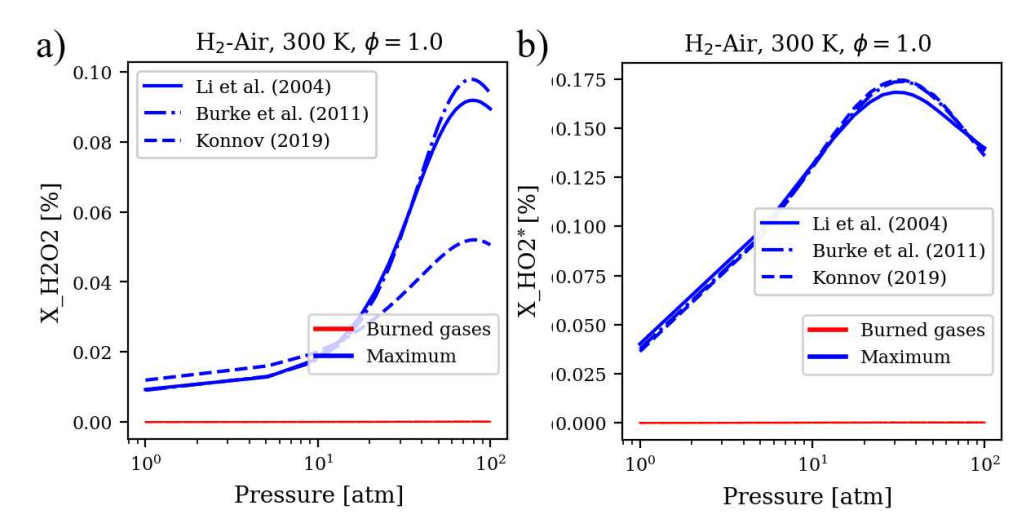


Figure 4.3 – H_2O_2 (a) and HO_2^* (b) species profiles for H_2 -air laminar premixed flames at $T_u = 300 \text{ K}$ and P = 1 to 100 atm.

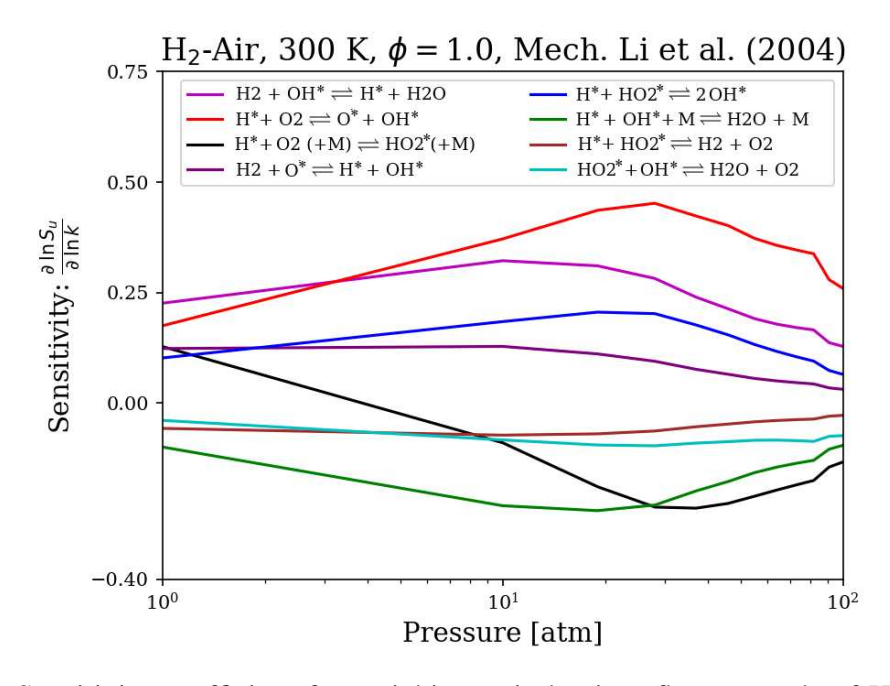


Figure 4.4 – Sensitivity coefficient for stoichiometric laminar flame speeds of H_2 -air at $T_u = 300$ K and P = 1 to 100 atm, Li *et al.* (2004) chemical kinetics mechanism.

Figure 4.5 presents ignition delay times (IDT) for H_2 -Air flames for 1-100 atm and initial temperatures between 1000 and 1667 K, showing a consistency between the three mechanisms predictions. For all pressures, the IDT value decreases with increasing temperature, but at 10, 50, and 100 atm the decrease is more pronounced than at atmospheric pressure. For the high-temperature limit of T=1667 K, IDT decreases for high-pressures of 10, 50, 100 atm relative to atmospheric pressure. At T=1000 K, IDT achieves maximum value at P=10 atm, and decreases for higher pressures of 50 and 100 atm, with minimum for 1 atm.

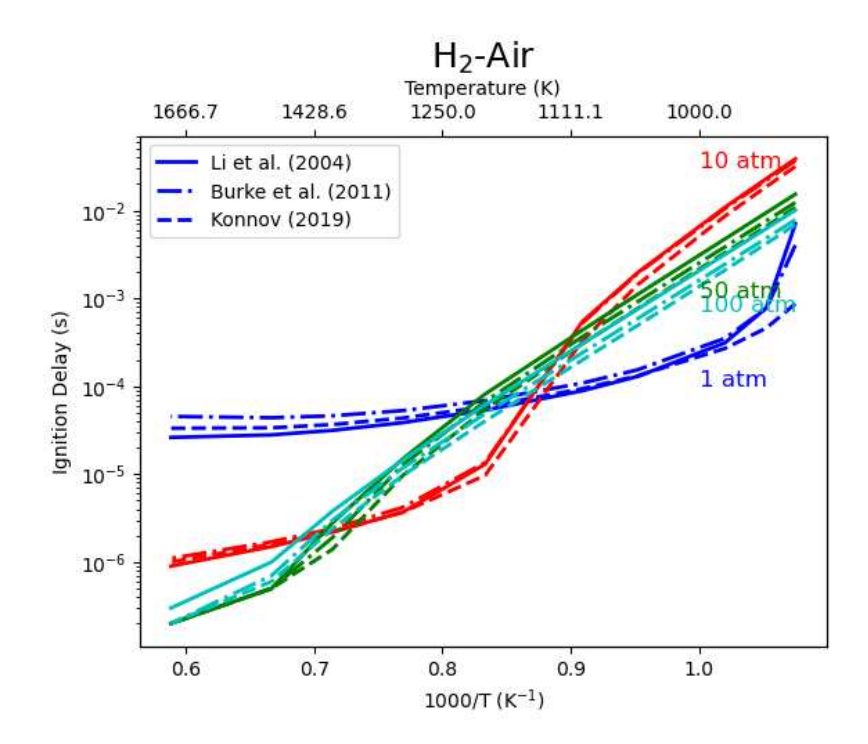


Figure 4.5 – Ignition delay times for stoichiometric H_2 -air mixtures at P=1 to 100 atm.

The analysis of hydrogen flames over a wide pressure range demonstrates a consistency of detailed chemical kinetics mechanisms in predicting laminar flame speeds, ignition delay times, and species profiles. The results highlighted the increasing role of pressure-dependent reactions, particularly the formation of HO₂*, in controlling flame propagation and reactivity at elevated pressures. While the radical pool of H*, O*, and OH* diminishes with pressure, HO₂* formation gains importance, contributing to the reduction in laminar flame speeds. These findings emphasize the fundamental chemical kinetics pathways governing hydrogen combustion under pressurized conditions and provide a reference framework for the development and validation of reduced chemical kinetics schemes in the following sections.

4.2 Supercritical combustion with real gas equation of state

4.2.1 Methods

For ultra-high pressure hydrogen flames calculations, a reduced version of the chemical kinetics mechanism of PLÁCIDO *et al.* (2024); PLÁCIDO (2024) was utilized, which accounts with 13 species and 37 reactions. The real-gas Peng-Robinson (PR) equation of state was utilized in Cantera 3.0 (GOODWIN *et al.*, 2023) for laminar flame speeds and ignition delay time calculations.

4.2.2 Results

Figures 4.6 and 4.7 show the profile of laminar flame speeds as a function of equivalence ratio results for ideal gas (IG) and Peng-Robinson (PR) equations of state (EoS) in ultra-high pressure conditions of P = 150to400 atm. It illustrates a notable deviation from ideal gas, which becomes increasingly pronounced with rising pressure in H₂-air flames: the PR EoS exhibits a maximum relative difference from the IG EoS of 4.3% at 150 atm and 16% at 400 atm. Overall, the PR EoS predicts higher values of LFS than the IG EoS under the simulated conditions. The normalized results highlights the deviation of the PR from the IG. The higher the combustion pressure the greater is the difference between the IG and PR LFS results. The highest differences starts near the stoichiometric point and it is less pronounced in lean flames. It is possible to note the importance of a real gas EoS as PR in the LFS for H₂-air flames calculation at high pressure, mainly for stoichiometric and rich flames.

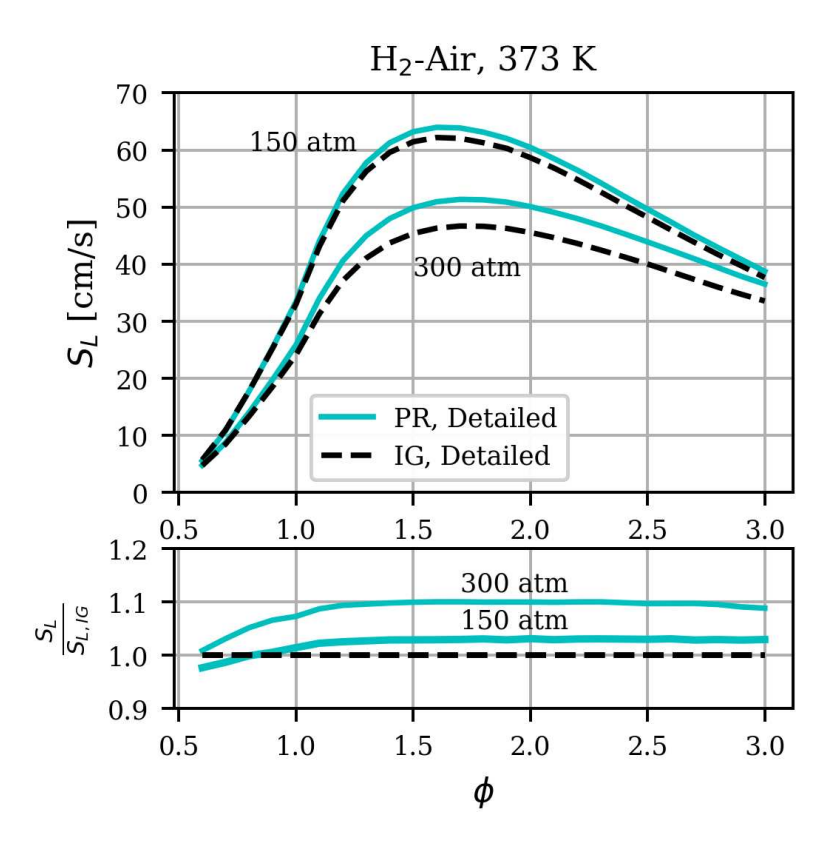


Figure 4.6 – Laminar flame speeds of H_2 -air mixtures for $T_u=373$ K, P=150 and 300 atm, comparing IG EoS and PR EoS.

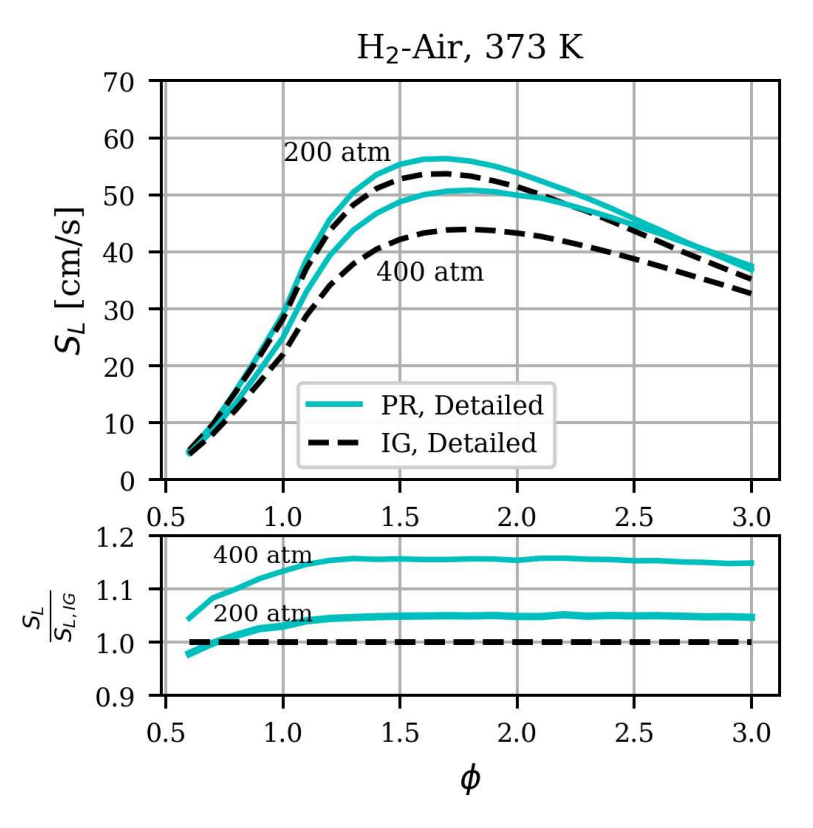


Figure 4.7 – Laminar flame speeds of H_2 -air mixtures for $T_u=373$ K, P=200 and 400 atm, comparing IG EoS and PR EoS.

Figure 4.8 shows IDT simulations for stoichiometric H_2 -air flames at P=100 and 300 atm, for initial temperatures (T_i) from 870 to 1250 K, comparing IG EoS and PR EoS, and Figure 4.9 for P=150 and 400 atm. The deviation of non-idealities becomes more pronounced with the pressure increase for IDT. The PR results present an IDT maximum relative difference from the IG of 5.4% at 100 atm, and of 17% at 400 atm.

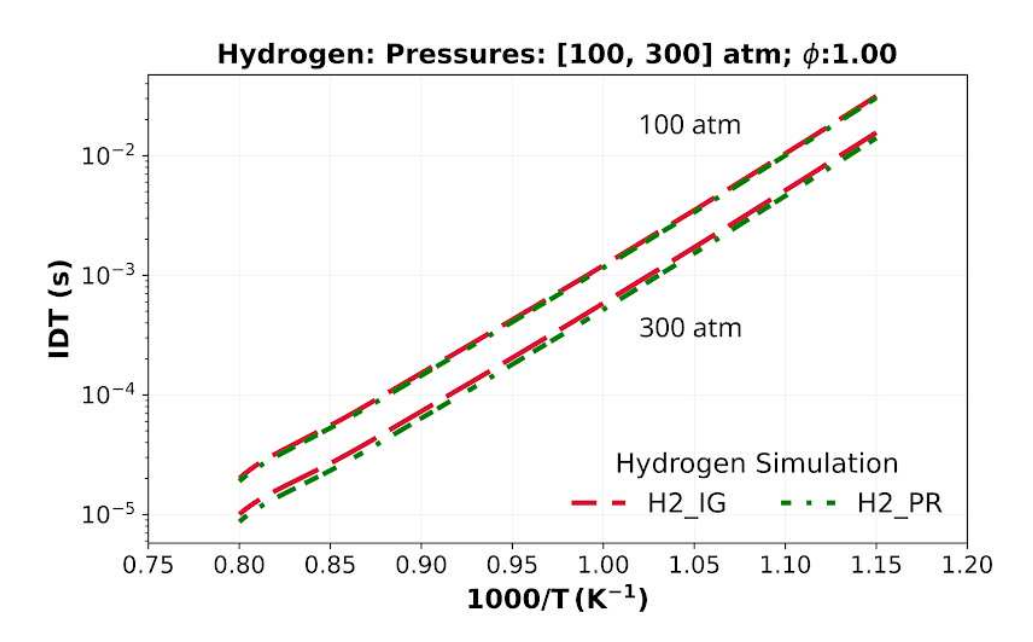


Figure 4.8 – Ignition delay time simulations for stoichiometric H_2 -air flames at P=100 and 300 atm, $T_i=870$ to 1250 K, comparing IG EoS and PR EoS.

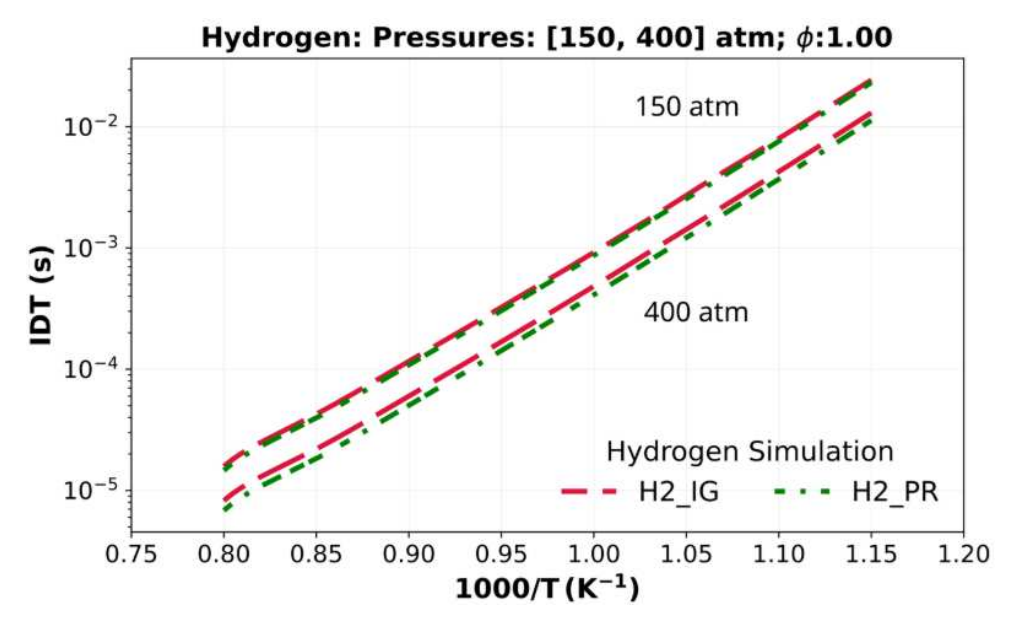


Figure 4.9 – Ignition delay time simulations for stoichiometric H_2 -air flames at P=150 and 400 atm, $T_i=870$ to 1250 K, comparing IG EoS and PR EoS.

Analyzing the temperature, gas density and species profiles of a freely-propagating, premixed hydrogen flat flame at 400 atm with PR and IG, in Figures 4.10, 4.11 and 4.12, respectively, it is possible to see differences. Using the PR EoS, the fresh gas density is about 14% lower than using the IG EoS. Also, the burned gas temperature is slightly lower with the real EoS. Species mass fraction profiles are also affected, lowering the O*, H*, and OH* radicals mass fractions in the burned gas composition. This indicates that the use of a real gas EoS as PR is important not only in the calculation of LFS or IDT at transcritical/supercritical conditions, but also in species calculations.

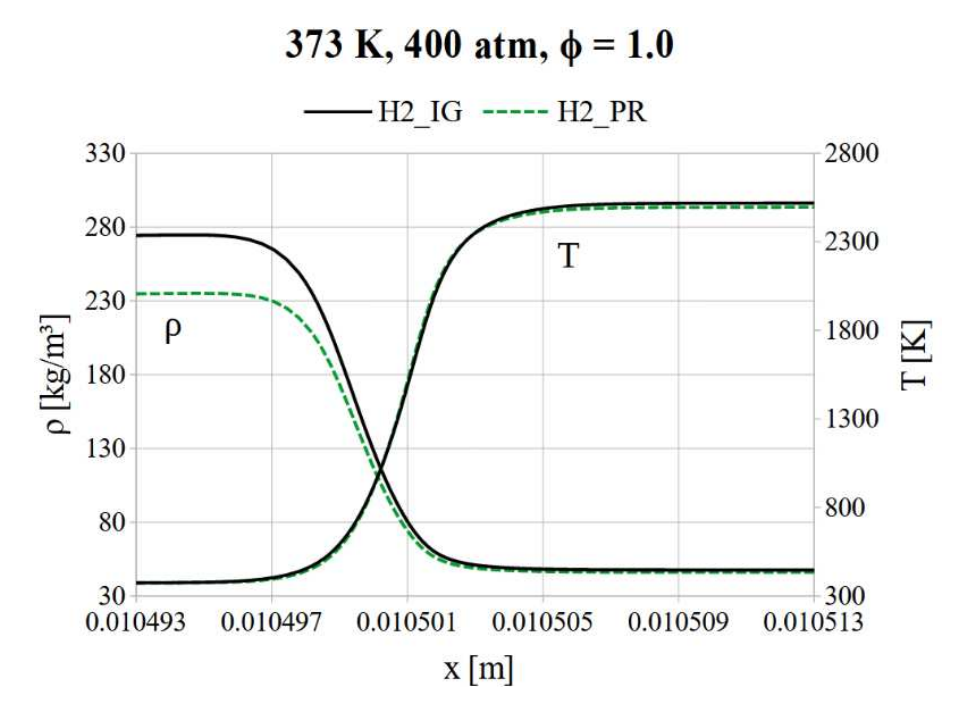


Figure 4.10 – Mixture gas density and temperature profiles of H_2 -air stoichiometric flames for $T_u = 373$ K, P = 400 atm, comparing IG EoS and PR EoS.

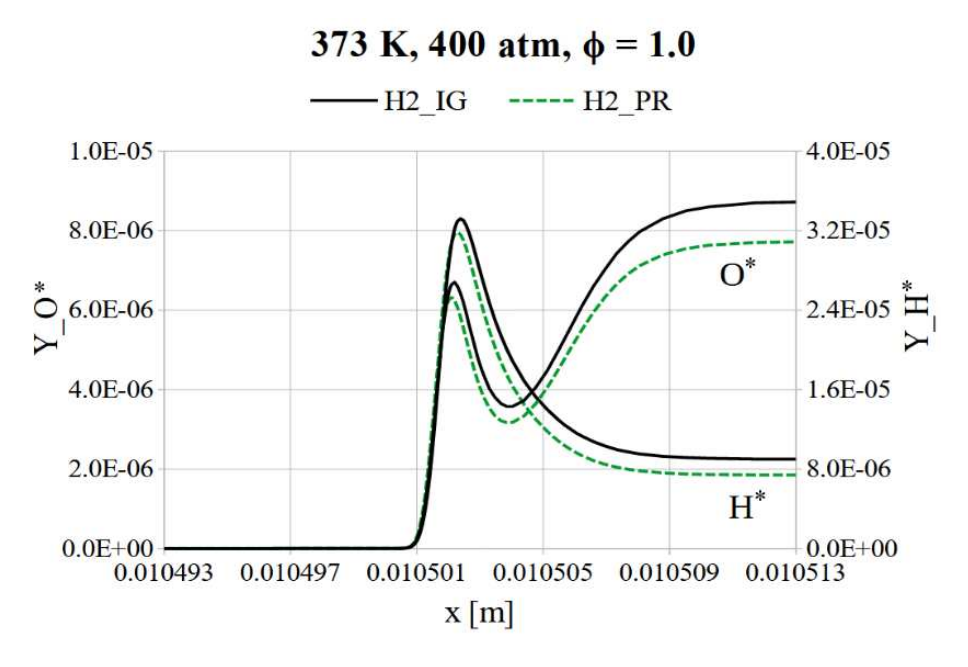


Figure 4.11 – O* and H* mass fraction profiles of H₂-air stoichiometric flames for T_u =373 K, P = 400 atm, comparing IG EoS and PR EoS.

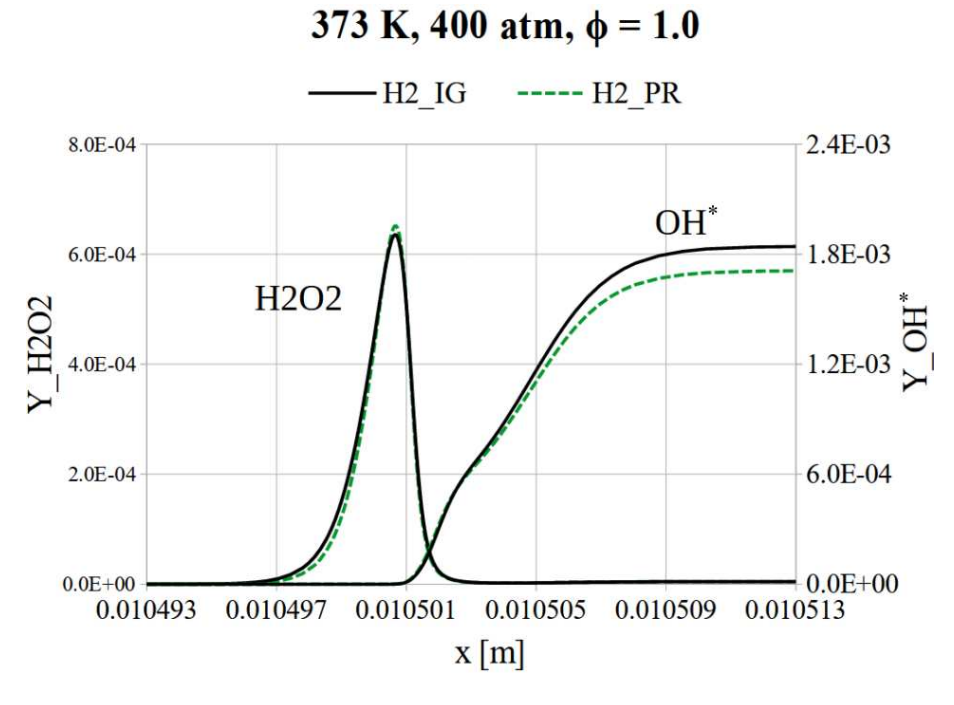


Figure $4.12 - \text{H}_2\text{O}_2$ and OH* mass fraction profiles of H₂-air stoichiometric flames for $T_u = 373 \text{ K}$, P = 400 atm, comparing IG EoS and PR EoS.

In summary, the comparison between the ideal gas and Peng-Robinson equations of state under ultra-high-pressure conditions demonstrated the increasing influence of real-gas effects on hydrogen combustion. Both laminar flame speed and ignition delay time results showed growing deviations with pressure, reaching nearly 20% at 400 atm. The analysis

of temperature, density, and species profiles further confirmed that non-ideal thermodynamic behavior affects not only global flame characteristics but also the radical pool and burned gas composition. These findings emphasize the importance of employing real-gas equations of state in the modeling of transcritical and supercritical combustion regimes, establishing a consistent framework for subsequent studies on reduced chemical kinetics mechanisms under such conditions.

4.3 Global chemical kinetics mechanisms

4.3.1 Methods

The one-step chemical kinetics mechanism can be represented by the reaction:

$$H_2 + O_2 \to H_2O,$$
 (4.1)

in which the reaction rate coefficient is given by:

$$k_f = AT^{\beta} e^{-\frac{E_{a,g}}{\mathcal{R}T}},\tag{4.2}$$

and production rate:

$$\dot{\omega} = k_f [H_2]^{n_F} [O_2]^{n_O}, \tag{4.3}$$

The genetic algorithm available in the python library Pygad (Gad, 2023) was used. Considering that an individual refers to a set of parameters - in this case A, $E_{a,g}$, β , n_F , n_O , called genes, a genetic algorithm is based on the evolution theory, in which the best individuals, are mantained for the next generation and go under operations called crossover and mutation than changes the genes values to form the new population, as represented in the flowchart of Fig. 4.13. The best individuals are chosen according to an objective/fitness function (GAD, 2018).

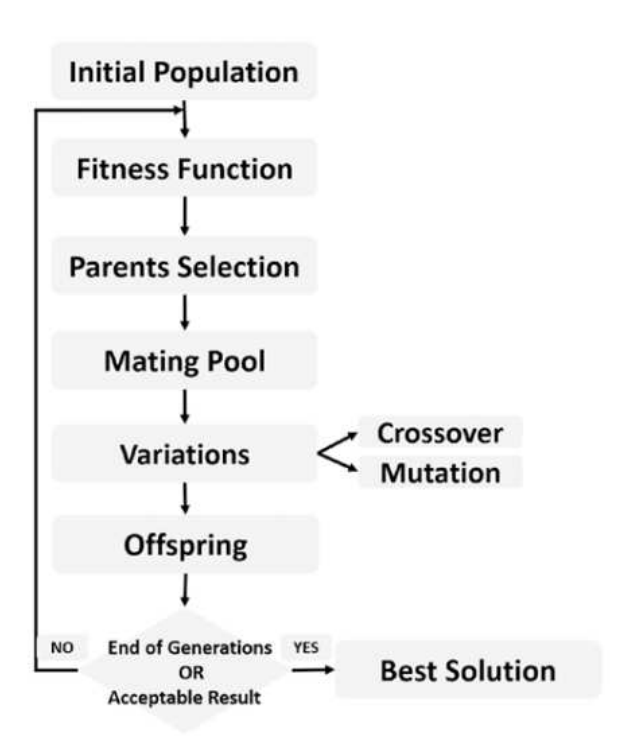


Figure 4.13 – Genetic algorithm flowchart. Source: GAD (2018).

4.3.2 Results

Table 4.2 presents the global chemical kinetics mechanism obtained at 1 atm, and Fig. 4.14 presents the laminar flame speeds for this condition, with the major deviation for lean mixture $\phi=0.6$ of 20%. Figure 4.15 presents the global mechanism performance at 1 atm for different mixture initial temperatures. It performed well for the temperature range of 100-600 K, particularly in the low to moderate temperature range, and the deviation increases slightly at higher temperatures where the global mechanism underpredicts stoichiometric mixture laminar flame speeds.

Table 4.2 – Global chemical kinetics mechanism for H_2 -air at $T_u = 300$ K and P = 1 atm.

P [atm]	$A\left[\frac{\mathrm{m}^3}{\mathrm{mol}^{p-1}\mathrm{s}}\right]$	$E_{a,g}\left[\frac{\mathrm{J}}{\mathrm{mol}}\right]$	n_F	n_O	β
1	3.14e+15	27745.0	0.57	0.67	-1.45

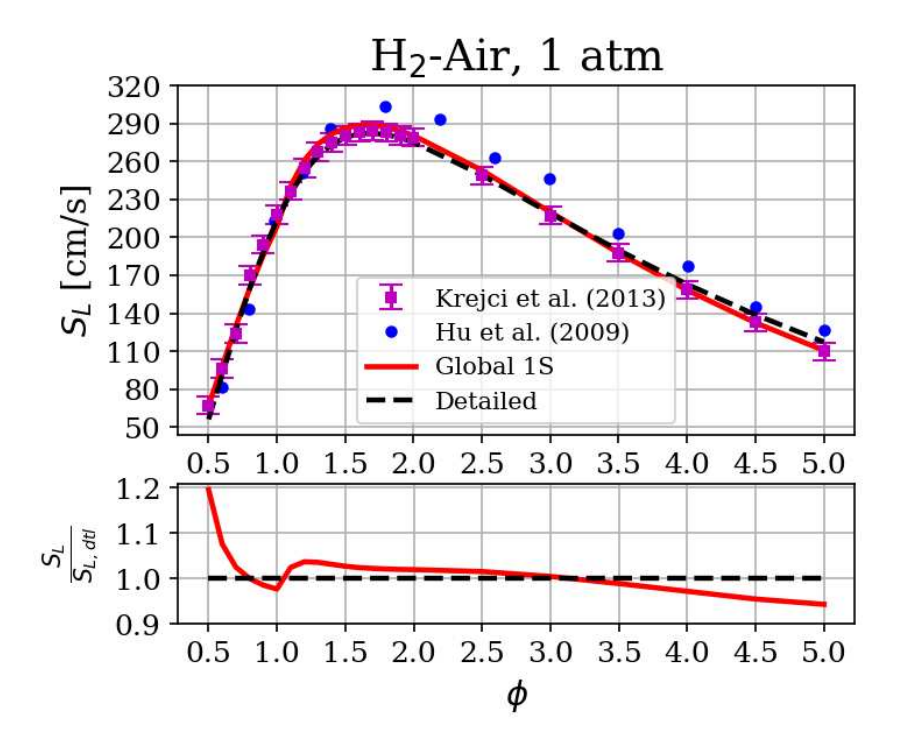


Figure 4.14 – Premixed hydrogen-air laminar flame speeds at $T_u=300~{\rm K}$ and $P=1~{\rm atm}$.

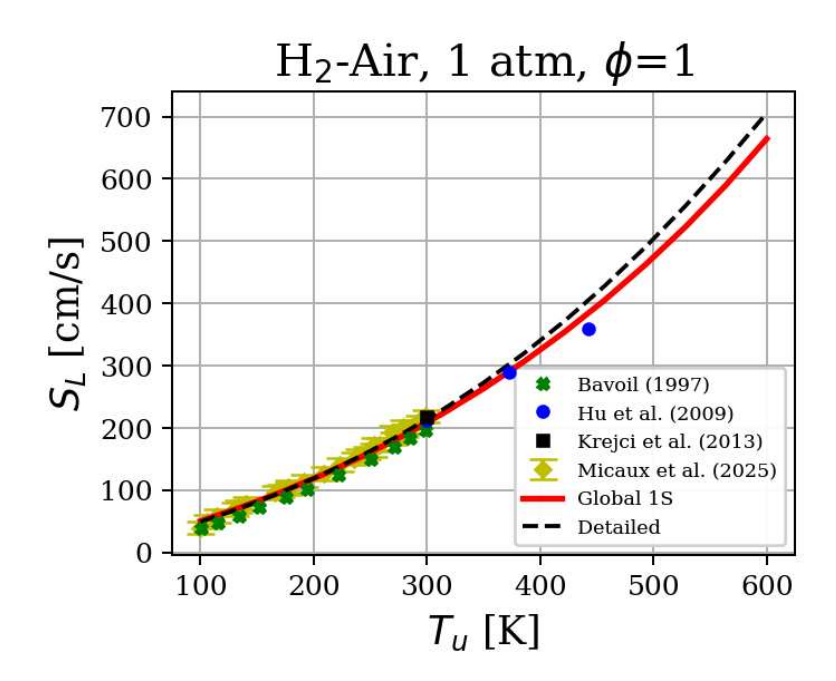


Figure 4.15 – Premixed hydrogen-air laminar flame speeds at P=1 atm and $T_u=100$ to 600 K.

Table 4.3 presents the global chemical kinetics mechanisms obtained for ultra-high-pressure combustion of hydrogen-air mixtures at the calibration pressure of 250 atm with the Peng-Robinson and the ideal gas equation of state. Figure 4.16 presents the laminar

flame speeds, with maximum deviation of 10% for lean ($\phi = 0.6$) and stoichiometric mixtures. Higher discrepancies were found using the mechanism for ideal gas than the mechanism calibrated using the Peng-Robinson EoS.

Table 4.3 – Global chemical kinetics mechanisms for H_2 -air at $T_u=300~{\rm K}$ and $P=250~{\rm atm}$.

Global chemical kinetics mechanisms, 250 atm							
EoS $A\left[\frac{\mathrm{m}^3}{\mathrm{mol}^{p-1}\mathrm{s}}\right]$ $E_{a,g}\left[\frac{\mathrm{J}}{\mathrm{mol}}\right]$ n_F n_O β							
Peng-Robinson	9.54e+19	46202.0	1.24	0.79	-1.28		
Ideal gas	3.01e+5	32023.0	1.56	1.27	3.62		

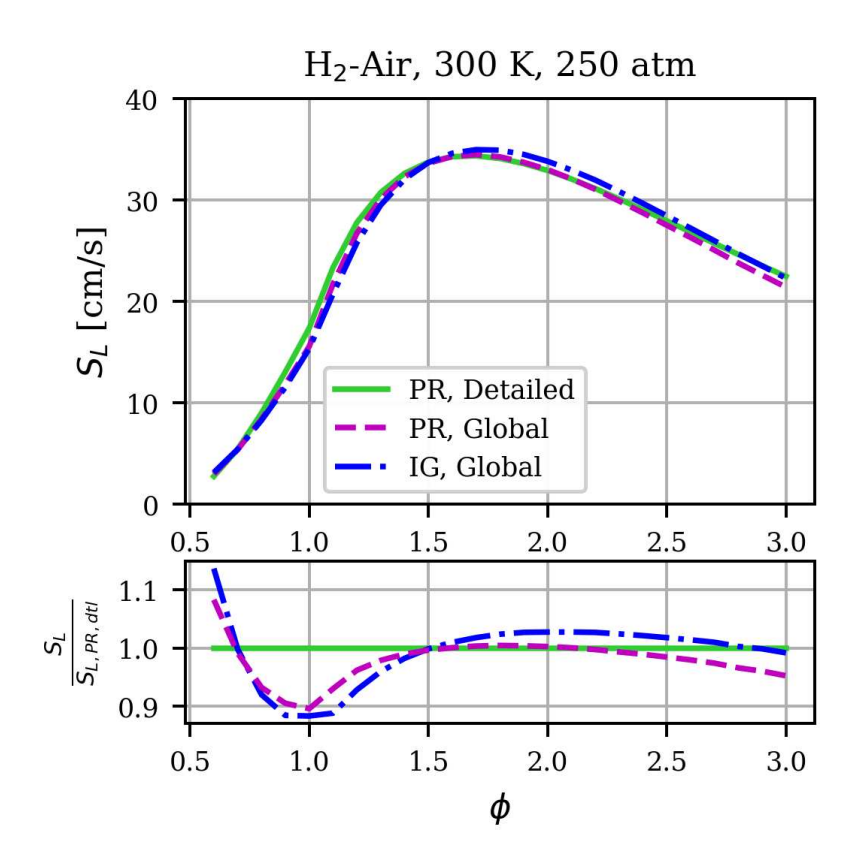


Figure 4.16 – Premixed hydrogen-air laminar flame speeds at $T_u=300~{\rm K}$ and $P=250~{\rm atm}$.

Tables 4.4 and 4.5 presents the global chemical kinetics mechanisms obtained for 200 and 300 atm, respectively, with the Peng-Robinson and the ideal gas equation of state. Figures 4.17 and 4.18 show a reasonable agreement, with maximum 20% difference for stoichiometric mixture at 200 atm, and 10% difference for stoichiometric and lean ($\phi=0.6$) at 300 atm, was achieved by adjusting the pre-exponential factor in relation to the value found at the calibration pressure 250 atm, as showed in Fig. 4.19; it was possible because the pre-exponential factor mainly shifted the LFS curve in the y-axis (LFS levels) under this pressure range.

Table 4.4 – Global chemical kinetics mechanisms for H_2 -air at $T_u=300~{\rm K}$ and $P=200~{\rm atm}$.

Global chemical kinetics mechanisms, 200 atm							
EoS $A\left[\frac{\mathrm{m}^3}{\mathrm{mol}^{p-1}\mathrm{s}}\right]$ $E_{a,g}\left[\frac{\mathrm{J}}{\mathrm{mol}}\right]$ n_F n_O β							
Peng-Robinson	1.08e+20	46202.0	1.24	0.79	-1.28		
Ideal gas	3.73e+5	32023.0	1.56	1.27	3.62		

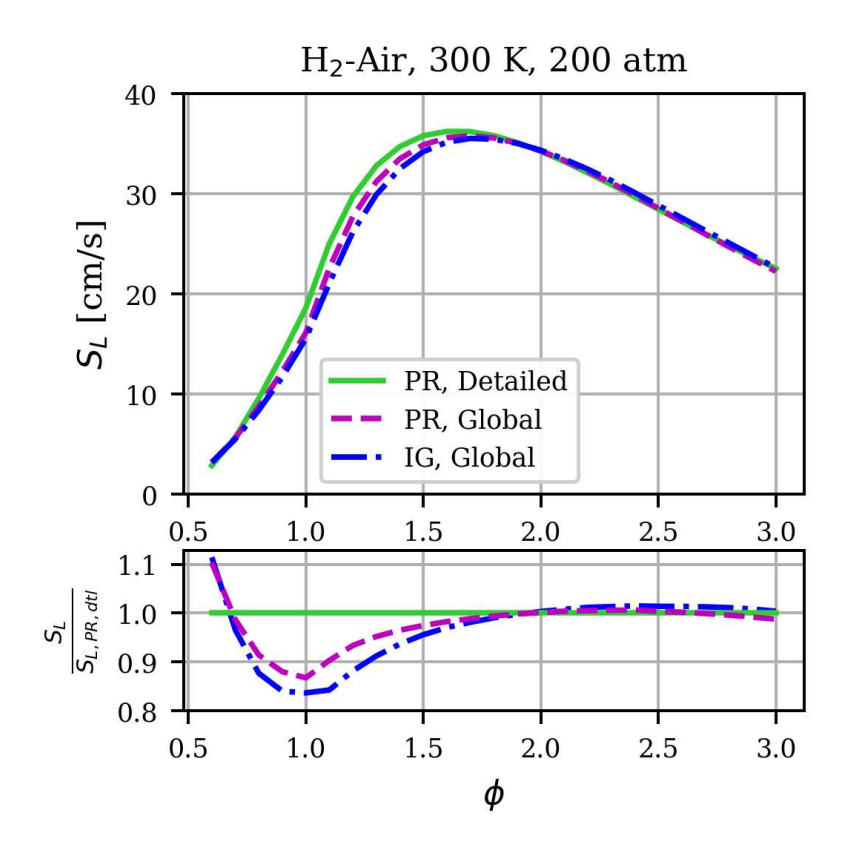


Figure 4.17 – Premixed hydrogen-air laminar flame speeds at $T_u=300~{\rm K}$ and $P=200~{\rm atm}$.

Table 4.5 – Global chemical kinetics mechanisms for H_2 -air at $T_u=300~{\rm K}$ and $P=300~{\rm atm}$.

Global chemical kinetics mechanisms, 300 atm							
EoS $A\left[\frac{\mathrm{m}^3}{\mathrm{mol}^{p-1}\mathrm{s}}\right]$ $E_{a,g}\left[\frac{\mathrm{J}}{\mathrm{mol}}\right]$ n_F n_O β							
Peng-Robinson	8.64e+19	46202.0	1.24	0.79	-1.28		
Ideal gas	2.41e+5	32023.0	1.56	1.27	3.62		

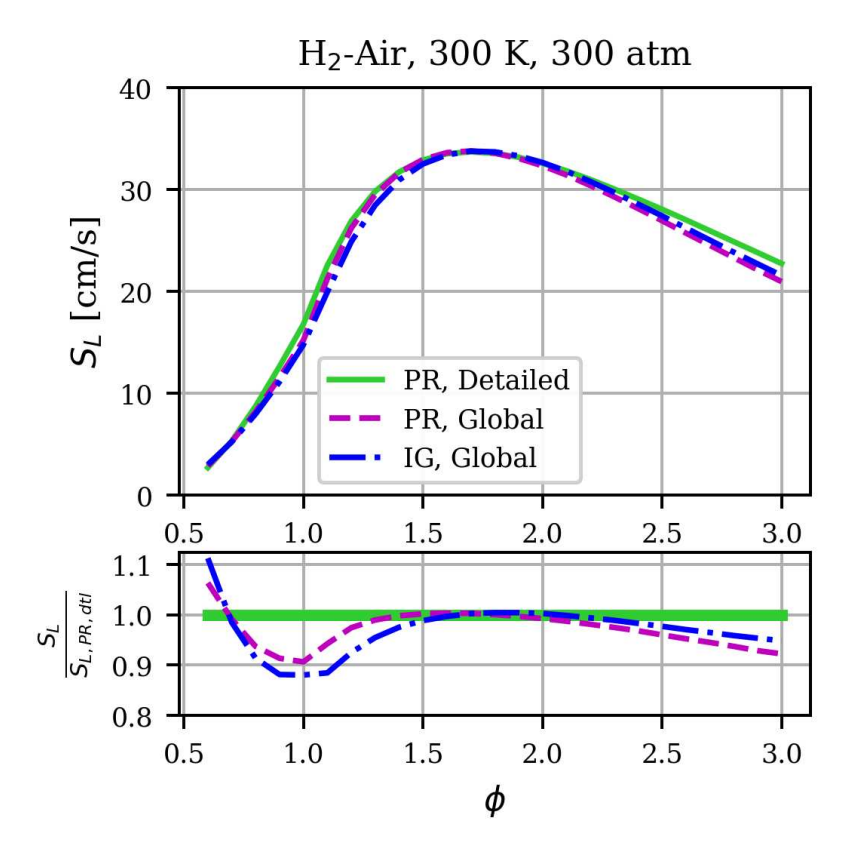


Figure 4.18 – Premixed hydrogen-air laminar flame speeds at $T_u=300~{\rm K}$ and $P=300~{\rm atm}$.

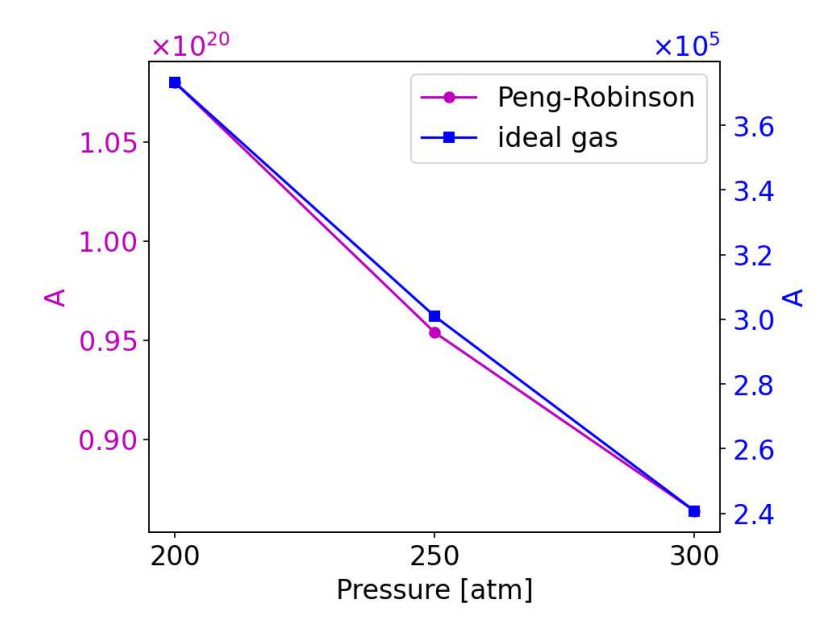


Figure 4.19 – Pre-exponential factor of the global kinetic mechanisms for $P=200,\,250,\,$ and 300 atm.

Although the global chemical kinetics mechanisms were calibrated to capture LFS, the predictions of temperature, density and molar fractions align closely to the detailed mechanism profiles at 250 atm (Fig. 4.20). However, Fig. 4.21 show that the global

mechanisms overpredicted the maximum heat release rate (HRR) in 10% for the lean mixture with $\phi=0.6$, and underpredicted in 20% for stoichiometric and rich ($\phi=3.0$) mixtures. Figure 4.22 show that IDT values were considerably underpredicted. The discrepancies in HRR and IDT predictions might be associated to the influence of intermediate and radical species on these quantities; higher discrepancies were found for the ideal gas global mechanism than the Peng-Robinson global mechanism, mainly for IDT.

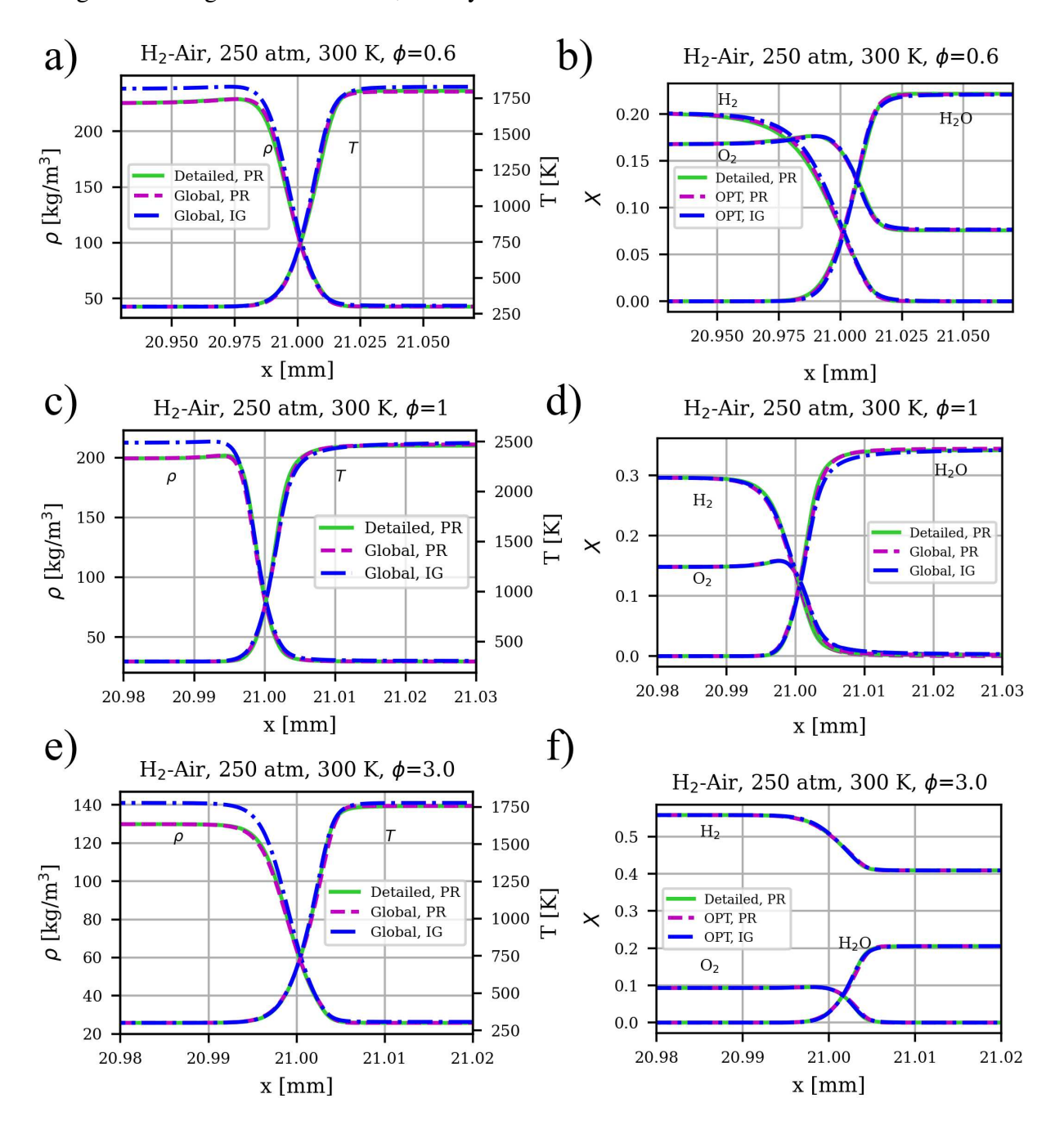


Figure 4.20 – Premixed hydrogen-air flame structure at $T_u=300$ K and P=250 atm for (a, b) $\phi=0.6$, (c, d) $\phi=1.0$, and (e, f) $\phi=3.0$.

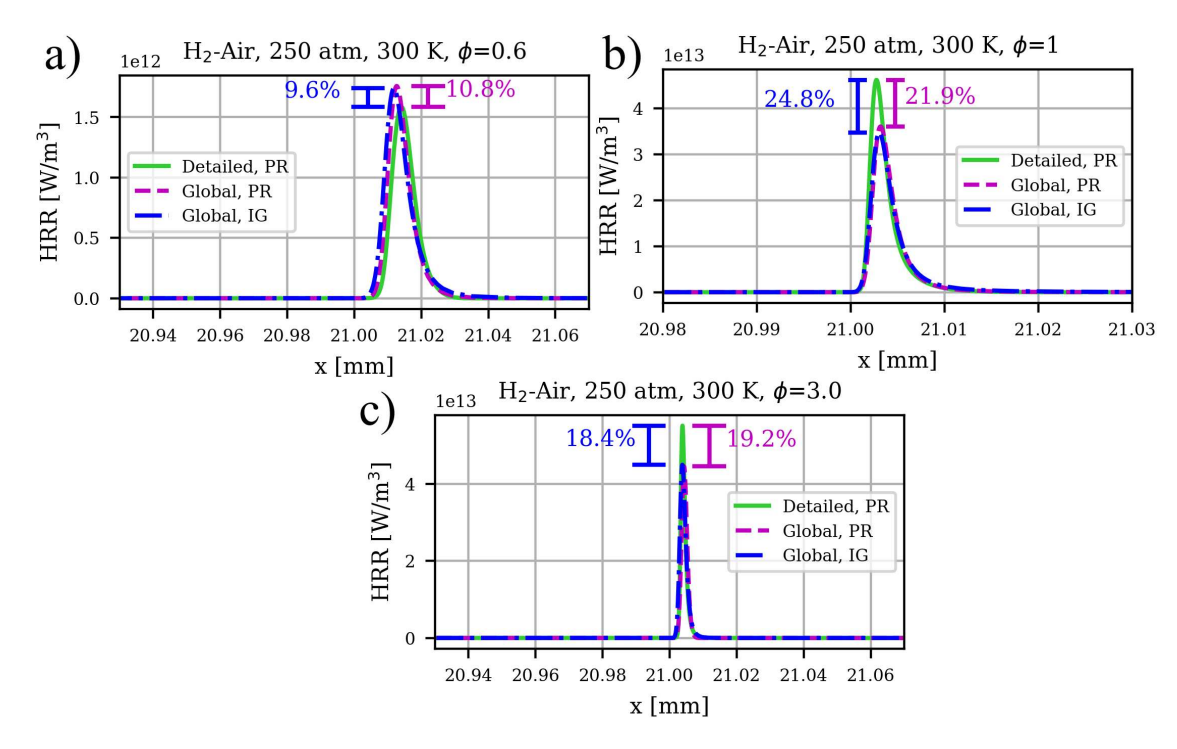


Figure 4.21 – Premixed hydrogen-air heat release rate profiles at $T_u = 300$ K and P = 250 atm for (a) $\phi = 0.6$, (b) $\phi = 1.0$, and (c) $\phi = 3.0$.

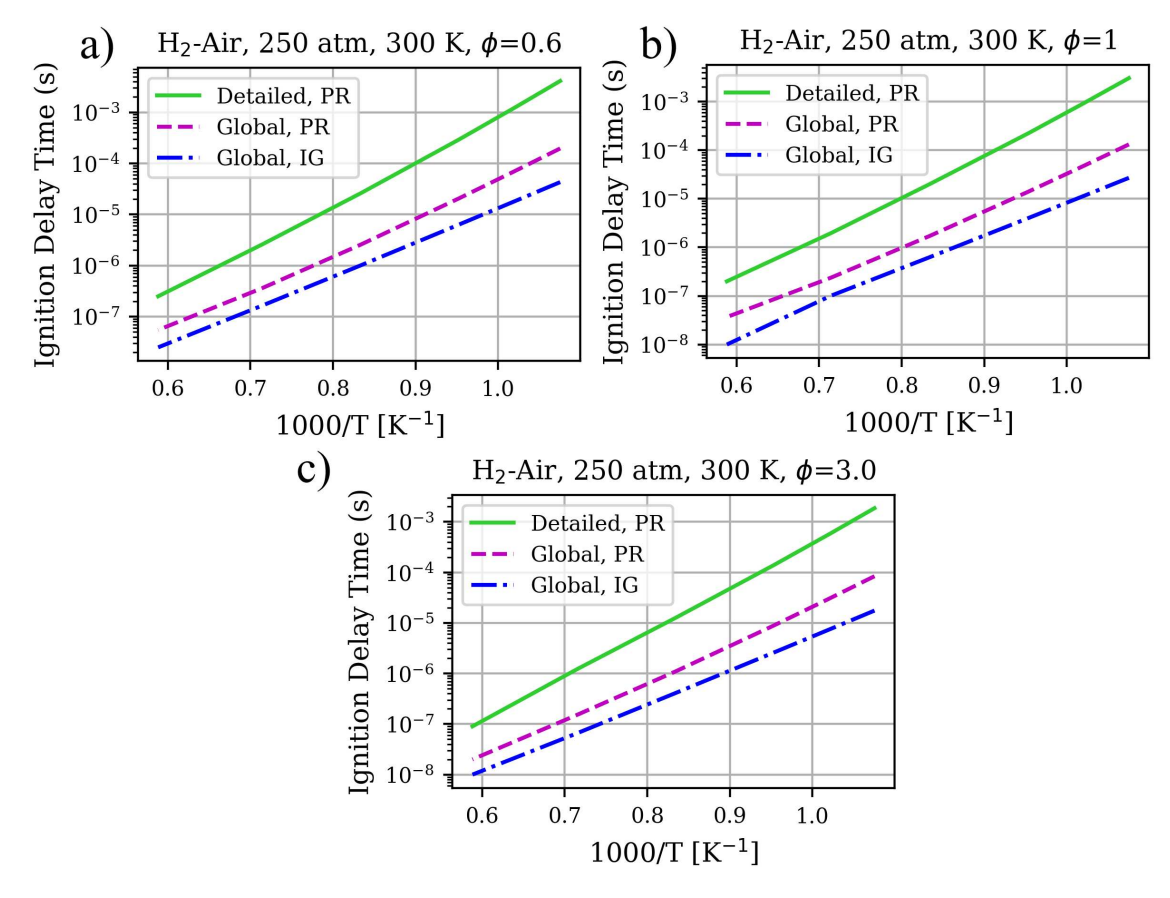


Figure 4.22 – Premixed hydrogen-air ignition delay time at P=250 atm for (a) $\phi=0.6$, (b) $\phi=1.0$, and (c) $\phi=3.0$.

5 CONCLUSIONS AND FUTURE WORKS

5.1 Conclusions

The development and validation of global chemical kinetics mechanisms for ethanol and hydrogen combustion demonstrated the capability of simplified models to accurately reproduce key combustion characteristics over a wide range of conditions. For ethanol, the two-step mechanism showed good agreement with both detailed chemical kinetics models and experimental laminar flame speed data, with deviations generally within ±5% and only reaching 10% under lean and rich limits conditions. Temperature profiles were also well predicted, with minor discrepancies attributed to the absence of intermediate and radical species in the global model, where endothermic effects from intermediate reactions reduce the maximum flow temperature. Furthermore, the mechanism maintained good predictive performance for stoichiometric mixtures over a broad range of initial temperatures (300–500 K), despite being optimized at 428 K.

the sensitivity analysis highlighted the importance For hydrogen, pressure-dependent reactions, such as the formation of HO₂, at high pressures. supercritical combustion, the non-ideal effects result in higher laminar flame speeds than the ideal gas. From 100 to 400 atm, the real fluid presents discrepancies from 4 to 16% relative to the ideal gas in predicting laminar flame speeds and ignition delay times. The PR EoS lowers the density of the fresh gas by 14% relative to IG, and also affects radical formation. The global mechanism provided good agreement with detailed models across varying equivalence ratios and temperatures at 1 atm, with the most significant deviation (20%) observed for lean mixtures. At ultra-high pressures the resulting flame speed predictions showed deviations below 10% at the calibration point (250 atm) and acceptable performance at neighboring pressures (200-300 atm), in which the mechanism was successfully calibrated by adjusting only the pre-exponential factor relative to the scheme obtained at 250 atm. While the flame structure was reasonably captured, the global models overpredicted heat release rates for lean $(\phi = 0.6)$ mixtures in 10% and underpredicted for stoichiometric and rich mixtures $(\phi = 3.0)$ in 20%. Ignition delay time was considerably underpredicted, which is related to the limitations of global mechanisms in capturing the detailed chemical kinetics associated with radical and intermediate species.

Overall, the global mechanisms developed in this study offer a computationally efficient yet physically consistent framework for simulating ethanol and hydrogen combustion. These models are particularly useful for large-scale simulations where detailed mechanisms are computationally prohibitive, although their limitations in applications where radical chemistry plays a dominant role.

5.2 Future works

This section summarizes some future works linked to this dissertation. The most important step is to verify the applicability of global chemical kinetics mechanisms, optimized to capture laminar flame behavior in one-dimensional simulations, in computational fluid dynamics codes and turbulent combustion simulations. Further, the methodology can be extended to other potential renewable fuels such as ammonia (NH₃), methanol (CH₃OH), and dimethyl ether (CH₃OCH₃). Other important investigation is on global chemical kinetics mechanisms capable of work with mixtures of those fuels.

BIBLIOGRAPHY

- ANAND, C.; Chandraja, B.; Nithiya, P.; Akshaya, M.; Tamizhdurai, P.; Shoba, G.; Subramani, A.; Kumaran, R.; Yadav, K. K.; Gacem, A.; Bhutto, J. K.; Alreshidi, M. A.; Alam, M. W. Green hydrogen for a sustainable future: A review of production methods, innovations, and applications. **International Journal of Hydrogen Energy**, v. 111, p. 319–341, 2025.
- BAGHERI, G.; RANZI, E.; PELUCCHI, M.; Parente, A.; Frassoldati, A.; Faravelli, T. Comprehensive kinetic study of combustion technologies for low environmental impact: Mild and oxy-fuel combustion of methane. **Combustion and flame**, v. 212, p. 142–155, 2020.
- BAI, J.; ZHANG, X.; ZHAO, H. Theoretical study of the real-fluid laminar flame propagation under supercritical conditions by using the virial equation of state and the enskog transport model. **Combustion and Flame**, v. 276, p. 114144, 2025.
- Burke, M.; Chaos, M.; Ju, Y.; Dryer, F.; Klippenstein, S. Comprehensive h2/o2 kinetic model for high-pressure combustion. **International Journal of Chemical Kinetics**, v. 44, p. 444 474, 07 2012.
- CAILLER, M. Virtual chemical mechanisms optimized to capture pollutant formation in turbulent flames. Tese (Theses) Université Paris Saclay (COmUE), Oct. 2018. Available at: https://theses.hal.science/tel-02283226>.
- CAILLER, M.; Darabiha, N.; Fiorina, B. Development of a virtual optimized chemistry method. application to hydrocarbon/air combustion. **Combustion and Flame**, v. 211, p. 281–302, 2020.
- CAILLER, M.; Darabiha, N.; Veynante, D.; Fiorina, B. Building-up virtual optimized mechanism for flame modeling. **Proceedings of the Combustion Institute**, v. 36, n. 1, p. 1251–1258, 2017.
- CRIPPA, M.; Guizzardi, D.; Pagani, F.; Banja, M.; Muntean, M.; Schaaf, E.; Monforti-Ferrario, F.; Becker, W.; Quadrelli, R.; Risquez Martin, A.; Taghavi-Moharamli, P.; Köykkä, J.; Grassi, G.; Rossi, S.; Melo, J.; Oom, D.; Branco, A.; San-Miguel, J.; Manca, G.; Pisoni, E.; Vignati, E.; Pekar, F. **GHG emissions of all world countries**. Publications Office of the European Union, 2024. JRC138862. Available at: https://edgar.jrc.ec.europa.eu/report_2024.
- EISAZADEH-FAR, K.; Moghaddas, A.; Al-Mulki, J.; Metghalchi, H. Laminar burning speeds of ethanol/air/diluent mixtures. **Proceedings of the Combustion Institute**, v. 33, n. 1, p. 1021–1027, 2011.
- FRANZELLI, B.; Riber, E.; Gicquel, L. Y.; Poinsot, T. Large eddy simulation of combustion instabilities in a lean partially premixed swirled flame. **Combustion and flame**, v. 159, n. 2, p. 621–637, 2012.
- FRANZELLI, B.; Riber, E.; Sanjosé, M.; Poinsot, T. A two-step chemical scheme for kerosene–air premixed flames. **Combustion and Flame**, v. 157, n. 7, p. 1364–1373, 2010.
- GAD, A. F. Practical Computer Vision Applications Using Deep Learning with CNNs: With Detailed Examples in Python Using TensorFlow and Kivy. 1. ed. Berkeley, CA:

- Apress, 2018. 405 p. Professional and Applied Computing, Apress Access Books. ISBN 978-1-4842-4166-0.
- Gad, A. F. Pygad: An intuitive genetic algorithm python library. **Multimedia Tools and Applications**, p. 1–14, 2023.
- GOODWIN, D. G.; Moffat, H. K.; Schoegl, I.; Speth, R. L.; Weber, B. W. Cantera: An Object-oriented Software Toolkit for Chemical Kinetics, Thermodynamics, and Transport Processes. 2023. Https://www.cantera.org. Version 3.0.0.
- GOODWIN, D. G.; Moffat, H. K.; Schoegl, I.; Speth, R. L.; Weber, B. W. Control Volume Reactor. 2025. https://cantera.org/dev/reference/reactors/controlreactor.html. Accessed: August 3, 2025.
- Goodwin, D. G.; Moffat, H. K.; Schoegl, I.; Speth, R. L.; Weber, B. W. **Ignition delay time using the Redlich-Kwong real gas model**. 2025. In: *Cantera: An object-oriented software toolkit for chemical kinetics, thermodynamics, and transport processes*, Version 3.1.0. Acesso em: 28 ago. 2025. Available at: https://cantera.org/dev/examples/python/reactors/non_ideal_shock_tube.html.
- Gupta, R.; Mishra, A.; Pathak, A. Supercritical Fluid technology a boon for pharmaceutical Particle Manufacturing. 2014.
- HONG, Z.; DAVIDSON, D. F.; HANSON, R. K. An improved h2/o2 mechanism based on recent shock tube/laser absorption measurements. **Combustion and Flame**, v. 158, n. 4, p. 633–644, 2011, special Issue on Kinetics.
- JOBACK, K. A unified approach to physical property estimation using multivariate statistical techniques. 08 2005.
- KATOCH, A.; Millán-Merino, A.; Kumar, S. Measurement of laminar burning velocity of ethanol-air mixtures at elevated temperatures. **Fuel**, v. 231, p. 37–44, 2018.
- KEE, R. J.; Coltrin, M. E.; Glarborg, P.; Zhu, H. Chemically reacting flow: theory, modeling, and simulation. [S.l.]: John Wiley & Sons, 2017.
- KILDARE, J. A.; Evans, M. J.; Tian, Z.; Medwell, P. R. Estimation and testing of single-step oxidation reactions for hydrogen and methane in low-oxygen, elevated pressure conditions. **Fuel**, v. 360, p. 130589, 2024.
- Konnov, A. A. Yet another kinetic mechanism for hydrogen combustion. **Combustion and Flame**, v. 203, p. 14–22, 2019.
- KROESE, D. P.; Rubinstein, R. Y. Monte carlo methods. **Wiley Interdisciplinary Reviews: Computational Statistics**, v. 4, n. 1, p. 48–58, 2012.
- Li, J.; Zhao, Z.; Kazakov, A.; Dryer, F. An updated comprehensive kinetic model of hydrogen combustion. **International Journal of Chemical Kinetics**, v. 36, p. 566 575, 10 2004.
- LIAO, S.; Jiang, D.; Huang, Z.; Zeng, K.; Cheng, Q. Determination of the laminar burning velocities for mixtures of ethanol and air at elevated temperatures. **Applied Thermal Engineering**, v. 27, n. 2, p. 374–380, 2007.

- Lu, X.; Hu, E.; Kokjohn, S.; Gao, Q.; Yin, G.; Zeng, K.; Huang, Z. Experimental and kinetic study of laminar flame characteristics of h2/o2/diluent flame under elevated pressure. **International Journal of Hydrogen Energy**, v. 45, n. 56, p. 32508–32520, 2020.
- LUCHE, J. Obtention de modèles cinétiques réduits de combustion-Application à un mécanisme du kérosène. Tese (Doutorado) Université d'Orléans, 2003.
- LV, Z.; CAO, H.; HAN, W.; Yang, L. Real-fluid effects on laminar premixed hydrogen flames under cryogenic and high-pressure conditions. **Combustion and Flame**, v. 272, p. 113837, 2025.
- MILLÁN-MERINO, A.; BOIVIN, P. A new single-step mechanism for hydrogen combustion. **Combustion and Flame**, v. 268, p. 113641, 2024.
- MIRA, D. **Towards high-fidelity combustion simulations**. 2024. https://www.youtube.com/watch?v=Co9Wk808_YI. Accessed: 2024-11-10.
- MITANI, T. Propagation velocities of two-reactant flames. **Combustion Science and Technology**, v. 21, n. 3-4, p. 175–177, 1980.
- NATIONAL AERONAUTICS AND SPACE ADMINISTRATION (NASA). **Global Temperature**. 2024. https://climate.nasa.gov/vital-signs/global-temperature/?intent=121. Accessed: 2025-03-02.
- NATIONAL INSTITUTE OF STANDARDS AND TECHNOLOGY. **NIST Standard Reference Database Number 69**. 2023. https://webbook.nist.gov/chemistry/#Documentation>.
- PETERS, N.; Rogg, B.; Williams, F. A.; Mauss, F. Reduced kinetic mechanisms for applications in combustion systems. [S.l.]: Springer Science & Business Media, 1993. v. 15.
- PLÁCIDO, P. V. R. Supercritical Combustion and Reduced Kinetic Modeling: Advancing Gasoline Surrogates/Ethanol Blends for Ultra-High-Pressure Conditions. Combustão Supercrítica e Modelagem Cinética Reduzida: Avanços em Combustíveis Substitutos de Gasolina/Etanol para Condições de Ultra-Alta Pressão. Tese (Tese de Doutorado em Engenharia Mecânica Térmica e Fluidos) Universidade Estadual de Campinas, Faculdade de Engenharia Mecânica, Campinas, SP, Brazil, 2024. Orientador: Prof. Dr. Rogério Gonçalves dos Santos. Coorientador: Prof. Dr. Dario Alberto Alviso Lopez.
- PLÁCIDO, P. V. R.; Alviso, D.; Santos, R. G. dos. A reduced kinetics model for the oxidation of transcritical/supercritical gasoline surrogate/ethanol mixtures using real gas state equations. **Combustion Science and Technology**, v. 0, n. 0, p. 1–27, 2024.
- POINSOT, T.; VEYNANTE, D. Theoretical and numerical combustion. [S.l.]: RT Edwards, Inc., 2005.
- PYTHON SOFTWARE FOUNDATION. **random Generate pseudo-random numbers**. [S.l.], 2024. Last updated: July 2024. Accessed: 2024-07-18. Available at: https://docs.python.org/3/library/random.html.
- RANZI, E.; Cavallotti, C.; Cuoci, A.; Frassoldati, A.; Pelucchi, M.; Faravelli, T. New reaction classes in the kinetic modeling of low temperature oxidation of n-alkanes. **Combustion and flame**, v. 162, n. 5, p. 1679–1691, 2015.

- RANZI, E.; Frassoldati, A.; Stagni, A.; Pelucchi, M.; Cuoci, A.; Faravelli, T. Reduced kinetic schemes of complex reaction systems: fossil and biomass-derived transportation fuels. **International Journal of Chemical Kinetics**, v. 46, n. 9, p. 512–542, 2014.
- RAU, F.; Hartl, S.; Voss, S.; Still, M.; Hasse, C.; Trimis, D. Laminar burning velocity measurements using the heat flux method and numerical predictions of iso-octane/ethanol blends for different preheat temperatures. **Fuel**, v. 140, p. 10–16, 2015.
- RENEWABLE FUELS ASSOCIATION. **Annual Ethanol Production**. 2025. https://ethanolrfa.org/markets-and-statistics/annual-ethanol-production. Accessed August 5, 2025.
- Ronan, P.; Pierre, B.; Christine, M.-R.; Guillaume, D.; Fabien, H. Laminar flame speed of ethanol/ammonia blends—an experimental and kinetic study. **Fuel Communications**, v. 10, p. 100052, 2022.
- SMITH, G. P.; Golden, D. M.; Frenklach, M.; Moriarty, N. W.; Eiteneer, B.; Goldenberg, M.; Bowman, C. T.; Hanson, R. K.; Song, S.; William C. Gardiner, J.; Lissianski, V. V.; Qin, Z. **WHAT'S NEW IN GRI-Mech 3.0**. 2000. http://www.me.berkeley.edu/gri_mech/>. Accessed: August 3, 2025.
- Su, B.; Papp, M.; Zhang, P.; Turányi, T. Dependence of ignition delay time on its definition a case study on methane ignition. **Combustion and Flame**, v. 262, p. 113364, 2024.
- TURNS, S. R. **Introduction to combustion**. 2. ed. [S.l.]: McGraw-Hill Companies New York, NY, USA, 1996.
- UNITED NATIONS CLIMATE CHANGE. **The Paris Agreement**. 2024. https://unfccc.int/process-and-meetings/the-paris-agreement. Accessed: 2025-03-02.
- WALTER, A.; DOLZAN, P.; Quilodrán, O.; de Oliveira, J. G.; da Silva, C.; Piacente, F.; Segerstedt, A. Sustainability assessment of bio-ethanol production in brazil considering land use change, ghg emissions and socio-economic aspects. **Energy Policy**, v. 39, n. 10, p. 5703–5716, 2011, sustainability of biofuels.
- WEEKES, R. T.; Nomura, K. K.; SÁNCHEZ, A. L.; WILLIAMS, F. A. A three-step reduced mechanism for mild combustion. **Combustion Science and Technology**, v. 195, n. 15, p. 3875–3881, 2023.
- WESTBROOK, C.; DRYER, F. Simplified reaction mechanisms for the oxidation of hydrocarbon fuel in flames. **Combustion Science and Technology**, v. 27, p. 31–43, 12 1981.
- ZHANG, Y.; WENG, Z.; MÉVEL, R. Laminar flame speeds of supercritical co2 diluted oxy-syngas and oxy-methane flames under direct-fired power cycle relevant conditions. **Combustion and Flame**, v. 266, p. 113526, 2024.
- ZHENG, L.; Figueroa-Labastida, M.; Nygaard, Z.; Ferris, A. M.; Hanson, R. K. Laminar flame speed measurements of ethanol, iso-octane, and their binary blends at temperatures up to 1020 k behind reflected shock waves. **Fuel**, v. 356, p. 129495, 2024.